

---

# Latent Concept Disentanglement in Transformer-based Language Models

---

Guan Zhe Hong<sup>\*1</sup> Bhavya Vasudeva<sup>\*2</sup> Vatsal Sharan<sup>2</sup> Cyrus Rashtchian<sup>3</sup>  
Prabhakar Raghavan<sup>3</sup> Rina Panigrahy<sup>3</sup>

<sup>1</sup>Purdue University <sup>2</sup>University of Southern California <sup>3</sup>Google Research  
hong288@purdue.edu, {bvasudev, vsharan}@usc.edu,  
{cyroid, pragh, rinap}@google.com

## Abstract

When large language models (LLMs) use in-context learning (ICL) to solve a new task, they seem to grasp not only the goal of the task but also core, latent concepts in the demonstration examples. This begs the question of whether transformers represent latent structures as part of their computation or whether they take shortcuts to solve the problem. Prior mechanistic work on ICL does not address this question because it does not sufficiently examine the relationship between the learned representation and the latent concept, and the considered problem settings often involve only single-step reasoning. In this work, we examine how transformers disentangle and use latent concepts. We show that in 2-hop reasoning tasks with a latent, discrete concept, the model successfully identifies the latent concept and does step-by-step concept composition. In tasks parameterized by a continuous latent concept, we find low-dimensional subspaces in the representation space where the geometry mimics the underlying parameterization. Together, these results refine our understanding of ICL and the representation of transformers, and they provide evidence for highly localized structures in the model that disentangle latent concepts in ICL tasks.

## 1 Introduction

Transformer-based Large Language Models (LLMs) demonstrate remarkable in-context learning (ICL) abilities: with only a handful of input-output demonstrations, they can generalize to new inputs without any parameter updates [1]. These successes hint that models might be inferring latent rules or concepts implicit in the prompt. Yet it is still unresolved whether transformers truly form explicit internal representations of such hidden structure, or whether apparent generalization can be explained by more superficial pattern matching. This work therefore asks:

*How do LLMs disentangle and manipulate latent concepts during in-context learning?*

Prior mechanistic studies leave this question open: most focus on tasks with simple latent structures which do not require intricate disentanglement nor manipulation of concepts. For instance, recent research has identified linear task or function vectors for problems such as basic arithmetic, single-step reasoning, and linguistic mappings [2, 3], and isolated certain attention heads that drive ICL behavior on these straightforward problems [4, 5, 6]. However, *real ICL usage often involves richer latent structures* — for instance, demonstrations with under-specified intermediate reasoning steps, or that share continuous latent parameters. It remains unclear how transformers *represent* these latent concepts, and how they *disentangle* and *reuse* them.

---

<sup>\*</sup>Equal contribution.

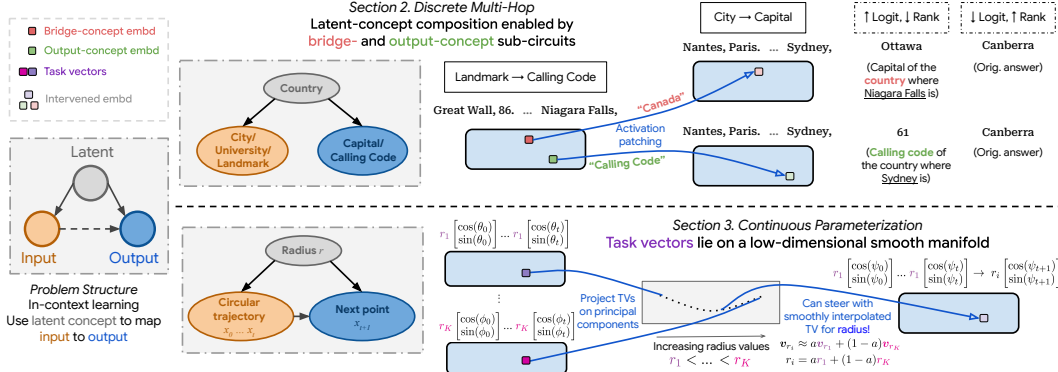


Figure 1: An illustration of problem setup and examples of main findings in this work. We primarily focus on how decoder-only transformer-based language models disentangle and manipulate latent concepts for solving in-context learning (ICL) problems. In the **multi-hop ICL** setting, we discover that transformers *compose* disentangled latent concept representations for predicting the answer. For example, as shown in the upper half of the figure, by intervening on certain “bridge-concept” attention heads, we can push the model’s “belief” (reflected in logit and rank) in the *original answer* Canberra (the capital of Australia, which the city Sydney belongs to) to the “type-corrected” *alternative answer* Ottawa (the capital of Canada, which the landmark Niagara Falls belongs to). In the **continuous-parameterization ICL** setting, we discover that transformers’ hidden embeddings capture the *geometry* of the latent concepts for our prediction tasks. For instance, for a transformer trained to predict circular trajectories whose radius is randomly chosen from a continuous interval, not only do we obtain causal evidence for *task vectors* which control the trajectory’s *radius*, but they also fall on a *smooth* 2D manifold.

We address these gaps by probing two challenging ICL settings:

- *Discrete multi-hop reasoning.* A model must map a “source” entity to a “target” entity (e.g., landmark→capital) by first latently inferring the hidden “bridge” entity (e.g., country), allowing us to ask whether the LLM first resolves the “bridge”, then refines it to a “target” entity via (causal) concept compositions.
- *Continuous-parameter tasks.* Demonstrations are generated by unknown real-valued parameters (e.g., the radius of a circular trajectory), allowing us to ask whether the model encodes such parameters along a systematic low-dimensional geometry.

Both tasks are *demanding enough* to require intricate latent concept disentanglement and manipulation, yet *sufficiently controlled* to permit causal, feature and circuit-level analysis.

Figure 1 illustrates the main ideas of our paper. Our experiments show that *transformers do learn, and when necessary, compose disentangled latent concept representations in these settings*. In the multi-hop task, we identify a highly sparse circuit of attention heads that first recovers the “bridge” concept, and then specializes it using “target concepts” to produce the answer. In the continuous tasks, we find that the model’s task vectors lie on a low-dimensional manifold precisely aligned with the underlying parameter. These results show that transformers internalize latent structure through specialized mechanisms rather than heuristics.

The remainder of this section details our task setups (Section 1.1) and summarizes our main contributions (Section 1.2).

## 1.1 ICL Tasks and Motivating Questions

We consider ICL problems involving (1) demonstration examples with *under-specified reasoning steps and latent, discrete concepts*, or (2) *latent, continuous parameterization*. These two structures comprise our two main investigation thrusts. For the first, we consider 2-hop factual recall tasks. For example, we give the model the name of a non-capital city and ask for the capital of the country containing this city. An instance looks like “Toronto, Ottawa. Sydney, Canberra. Mumbai, New Delhi. Shanghai, ”, where the final answer is Beijing. The motivation here

comes from understanding what the model does *after* reading the input city. Does it jump directly to the capital, or does it first invoke the country as an intermediate reasoning step? While both are sensible solution strategies, only the latter captures the latent causal structure that goes through the latent variable (the country).

The second part of our work examines ICL tasks with a latent, continuous parameterization. First, we consider an *add-k* task (also studied by [7]) where the demonstration examples are  $(x_i, y_i)_{i=1}^n$  with  $y_i = x_i + k$ , where  $k$  is the latent parameter. Given this context, the model needs to make a prediction for a test point  $x_{n+1}$ . An example of add-4 is “5, 9. 3, 7. 1, 5. 2, ”, where the answer is 6. To generalize from this linear offset setting, we also consider in-context tasks with simple geometric structure, such as a Circular-Trajectory task with data lying on a circle with varying radii. Our goal across these tasks is to localize the task vector in the model, and more importantly, understand the geometry of the task vectors. Do the task vectors for different values of the underlying continuous parameter lie in some low-dimensional space, and exhibit relations which reflect the parameterization? While previous work has investigated the presence of task vectors in such tasks, the structure latent in these task vectors has not achieved much attention.

## 1.2 Main Contributions

We provide mechanistic evidence of the transformer capturing the underlying concept structure, on discrete ICL problems involving latent 2-hop reasoning, and those with continuous parameterization.

For the 2-hop setting, we focus on the Gemma 2 family of LLMs [8]. We make the following discoveries:

- For the largest 27B model, we find that it uses a *step-by-step composition of latent concept representations* to answer the query. In particular, we discover that a highly sparse set of attention heads is responsible for resolving the intermediate latent concept (e.g., the country when going from city to capital). Then, we show that there is another set of heads deeper in the model responsible for realizing the concrete output (such as the capital) from the intermediate concept. We characterize the nuances of these inference mechanisms, providing both correlational and causal evidence for their functionality.
- We also show that as the number of in-context examples increases, model accuracy, causal importance of the circuit which invoked the intermediate concept, and concept representation disentanglement all increase.
- In contrast to the large 27B model, we find that the smaller 2B variant (having much lower accuracy) contains a much *weaker and noisier* version of the 27B model’s circuit, suggesting that model size significantly impacts concept disentanglement and composition abilities in the LLMs.

Since our tasks with latent *continuous* parameterization – such as add- $k$  and Circular-Trajectory – do not require world knowledge, we train two-layer models on which we can conduct a more controlled analysis by training from scratch on the task.

- Our key finding is that the models not only have task vectors, but these representations *reflect the geometry of the latent variable*. For example, the task vectors for add- $k$  almost entirely project onto a line, and interpolating along this line approximately interpolates on the latent parameter  $k$  for the task.
- For the Circular-Trajectory task, we see a similar geometry in a 2-dimensional space. This aligns with the linear representation hypothesis, but provides more nuanced evidence for it by showing a more continuous parameterization along the representation direction. As with the 2-hop task, we provide evidence through both correlational analysis and localization of task vectors in the model’s representation.

Together, these results provide new insights into in-context learning in multiple settings. Across our two types of tasks, we show that models encapsulate the latent structures of the tasks they learn in context. Moreover, the disentangled structures are surprisingly interpretable and highly localized in the model — a sparse set of attention heads disentangles the 2-hop reasoning tasks, and a one or two dimensional subspace in the representation captures the add- $k$  or Circular-Trajectory task. This raises the possibility that LLMs can more broadly identify and reuse latent concepts in an interpretable way.

## 2 Disentanglement for Latent Discrete Task in Multi-hop Reasoning

Prior works have mechanistically analyzed how LLMs solve ICL problems that require a single step of reasoning over world knowledge, such as geography puzzles “Country→Capital”, “National Park→Country” [2, 5]. However, whether and how LLMs can solve ICL problems with *underspecified reasoning steps*, or essentially those requiring *latent multi-hop reasoning* remains unclear.

**The “Source→Target” problem.** We create two-hop ICL puzzles by composing two facts linked by a common “Bridge” entity.<sup>2</sup> That is, we sample fact tuples  $\{(S_i, r_1, B_i, r_2, T_i)\}_{i=1}^n$ , where the Source entity  $S_i$  is related to the Bridge entity  $B_i$  via relation  $r_1$ , and  $B_i$  is related to the Target entity  $T_i$  via  $r_2$ . We then create the ICL puzzle in the form  $[S_1, T_1. S_2, T_2 \dots S_n, T_n]$  [Answer:  $T_n$ ]. Note that the bridge entities  $B_i$ ’s are never specified in the prompt. In the main text, we primarily work with geography puzzles,<sup>3</sup> with input types {City, University, Landmark}, and output types {Capital, Calling code}. An example problem is

Sydney, Canberra. Nantes, Paris. Oshawa,

Here,  $r_1$  is “belongs to the country of”, the (unspecified) bridge entities for this example are “Australia”, “France”, “Canada”, and  $r_2$  is “has capital”. Therefore, the prompt’s answer is Ottawa, the capital of Canada, the country Oshawa is in.

We begin our analysis by testing Gemma-2-27B on these ICL puzzles. We report the model’s accuracy in Figure 2. While the model apparently struggles more on these problems than on the simpler one-hop counterparts due to a greater demand for in-context examples, it does achieve high accuracy at 20 shots.

This raises several questions. How is the LLM solving these harder, “source→target” problems that *do not specify the bridge, or even hint at the compositional nature of the problem at all*? Given sufficiently many in-context examples, does a sufficiently capable LLM latently infer the bridge value when it sees the query and predicts the answer? How does the number of in-context examples impact the model’s inference mechanisms?

In the following, we show evidence suggesting that the model indeed performs latent multi-hop reasoning, in the form of sequential “*concept composition*”: it first infers an abstract “bridge” concept representation (e.g. a “Canada” concept), then specializes to a specific output trait (e.g. the “capital” of “Canada”) deeper in the model. We find that this mechanism gradually strengthens in its dominance of the model’s inference pathway as the number of ICL examples increases.

A surprising finding is that a highly sparse set of attention heads are responsible for “resolving the bridge value”. For example, on these heads, if we patch the representation of a “calling code” prompt such as “Shenzhen, 86. Nantes, 33. Oshawa, ” [Bridge = Canada] onto their representation of the “capital” prompt “Lausanne, Bern. Okinawa, Tokyo. Florence, ” [Output Concept = Capital], then the model turns to place significant confidence on “Ottawa” (“Capital” of “Canada”)!

### 2.1 Experimental Set-up

**LLM choice.** In the main text, we primarily focus on presenting interesting core results for the Gemma-2-27B model [8] in consideration of limited space, and delay nuanced circuit analysis results of the model and other LLMs to Appendix A.

**The “source→target” puzzles.** We collect the puzzles’ data for over 40 countries in the world. For each source type in {City, University, Famous Landmark}, we collect at least 10 entities per country,

<sup>2</sup>We think of this as a systematic ICL version of TWOHOPFACT [9]. Here, the model must figure out relations between the *input-bridge* and *bridge-output* facts from the ICL examples.

<sup>3</sup>We report on other LLMs and problem types in Appendix A.

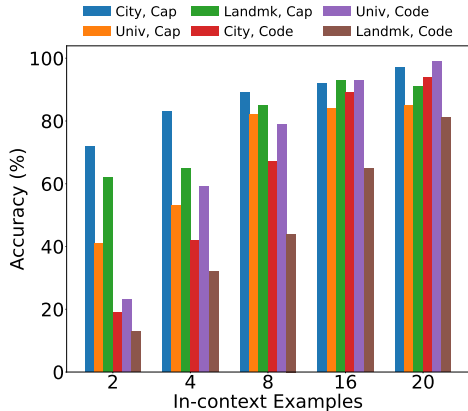


Figure 2: Accuracy of Gemma-2-27B on the two-hop “Source→Target” ICL problems.

leading to over 400 possible source entities per source type in the puzzles. We detail our full dataset (including other puzzle types) in Appendix A.1 and A.3.

**Causal Mediation Analysis.** We rely on causal mediation analysis (CMA), a.k.a., activation patching [10, 11] to obtain causal evidence for our claims. It is suitable to our problem setting, as it enables us to localize components inside the LLM which specialize in handling the different (latent) reasoning steps of the problem. Formally, given normal and altered prompt pairs  $\mathbf{p}_{\text{norm}} = [S_1^{(\text{norm})}, T_1^{(\text{norm})} \dots S_n^{(\text{norm})}]$  and  $\mathbf{p}_{\text{alt}} = [S_1^{(\text{alt})}, T_1^{(\text{alt})} \dots S_n^{(\text{alt})}]$ , we run the LLM on both prompts and cache the LLM’s hidden activations, denoted as  $(\mathbf{h}_{\text{norm}}, \mathbf{h}_{\text{alt}})$ .

To perform CMA on a model component of interest, say an attention head with activations indexed by  $(\mathbf{a}_{\ell, h}^{(\text{norm})}, \mathbf{a}_{\ell, h}^{(\text{alt})})$ , we run the LLM on the normal prompt again, but this time, intervene by replacing its normal activation by the altered  $\mathbf{a}_{\ell, h}^{(\text{alt})}$ , and let the rest of the causal graph execute. We then examine the model’s output behavior on the normal and patched runs, by, for example, examining the logit difference between the normal and altered answers. More specifically, we examine the (expected) *intervened* logit difference

$$\Delta_{\text{alt} \rightarrow \text{norm}} = \mathbb{E} \left[ \text{logit}^{\text{alt} \rightarrow \text{norm}}(\mathbf{p}_{\text{norm}})[T_n^{(\text{norm})}] - \text{logit}^{\text{alt} \rightarrow \text{norm}}(\mathbf{p}_{\text{norm}})[T_n^{(\text{alt})}] \right], \quad (1)$$

versus the *natural* (un-intervened) logit difference on the normal prompts

$$\Delta_{\text{norm}} = \mathbb{E} \left[ \text{logit}(\mathbf{p}_{\text{norm}})[T_n^{(\text{norm})}] - \text{logit}(\mathbf{p}_{\text{norm}})[T_n^{(\text{alt})}] \right]. \quad (2)$$

The *logit-difference variation* is computed by

$$\bar{\Delta} = \frac{\Delta_{\text{norm}} - \Delta_{\text{alt} \rightarrow \text{norm}}}{\Delta_{\text{norm}}}, \quad (3)$$

where  $\text{logit}^{\text{alt} \rightarrow \text{norm}}(\mathbf{p}_{\text{norm}})$  is obtained by replacing the activation of a chosen model component (e.g.  $\mathbf{a}_{\ell, h}^{(\text{norm})}$  for a chosen  $(\ell, h)$  tuple) on the normal prompt  $\mathbf{p}_{\text{norm}}$  by its counterpart obtained on the alternative prompt. We omit specific intervened model-component indices in the equations for notational simplicity here.

For a well-performing model,  $\Delta_{\text{norm}}$  should clearly be a large positive number on average. On a patched run, if certain components have strong causal influence on the model’s inference of the right answer,  $\Delta_{\text{alt} \rightarrow \text{norm}}$  should then be bent towards the negative. In addition to logit difference, when it makes sense, we also directly examine the (reciprocal) rank of the normal and altered answer before and after patching. We delay formal discussions of CMA (and the metrics), and its suitability to our problem to Appendix A.1.

## 2.2 Correctly answering the query: step-by-step composition of concept representations

We next analyze how the LLM infers the answer (target entity) from the query (source entity), given sufficiently many in-context examples. We will show both causal and correlational evidence that the LLM latently infers the bridge entity as an abstract concept representation, and compose it with output-concept representations to produce the answer. To achieve this, there are two main steps of our experiments, which we discuss below.

**Step 1: bridge-resolving attention heads.** We perform activation patching (CMA) on normal and altered problem pairs with different bridge entities (different countries), across different source and target types, at the last token position. If our hypothesis of certain attention heads resolving the bridge value from  $S_n$  for prediction is correct, then this bridge representation must be *transferable across source and target types*: for instance, patching a [University→Calling Code] prompt’s activation (i.e., activations on the alternative prompt) onto that of a normal prompt [City→Capital], should cause the model to favor the alternative prompt’s answer, but in the form of Capital (instead of Calling Code).

This suggests a slightly unorthodox intervention experiment. Instead of taking the normal-alternative answer pairs to be the ground truths, *we convert the alternative answer into the same output/target type as the normal one*, i.e., set  $\hat{T}_n^{(\text{alt})} = \text{Type}_{\text{norm}}(T_n^{(\text{alt})})$ . The logit difference and (reciprocal) rank of the alternative answer would use the *type-corrected*  $\hat{T}_n^{(\text{alt})}$  instead of the raw target  $T_n^{(\text{alt})}$ . For

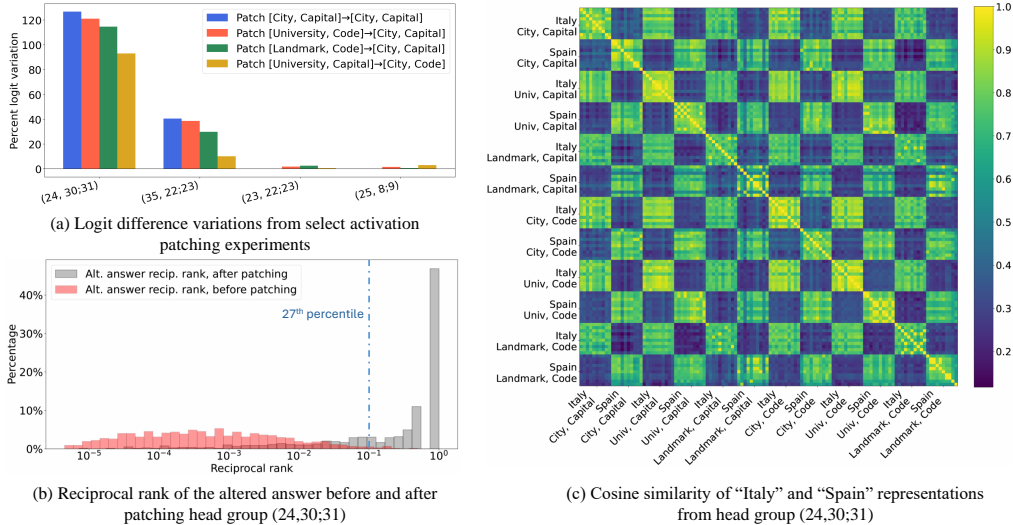


Figure 3: Evidence of the bridge-resolving attention heads in Gemma-2-27B. We present causal evidence for the bridge-resolving mechanism in (a) and (b), and correlational evidence in (c). In (a) and (b), we run activation patching experiments across prompts with problems of different source and target types, at the final token position. (a) shows the percentage logit difference variation of attention heads with the strongest causal influence, on select intervention experiments. Head group (24,30;31)’s representation exhibits strong transferability across source and target types. (b) further examines the causal role of (24,30;31), in the patching experiment [University, Code]→[City, Capital]. Note that the reciprocal rank of  $10^{-1}$  for the type-corrected alternative answer after patching (24,30;31) is in the 27th percentile ( $> 73\%$  in top 10 after intervention). In (c), we show a cosine similarity plot of bridge-representation disentanglement for head group (24,30;31), computed on a collection of samples with with several combinations of source and target types, and with “Italy” and “Spain” as the bridge values in the prompts.

instance, if the normal prompt is “Shanghai, Beijing. Busan, Seoul. ... Birmingham, ” which has target type *Capital*, and the alternative prompt is “Nagoya University, 81. ... EPFL, ” [Answer  $T_n^{(alt)} = 11$ ], then  $\hat{T}_n^{(alt)} = \text{Bern}$ , the same target type as the normal prompt (*Capital*), but with the same bridge as the alternative prompt (Switzerland).

We report the results in Figure 3: this figure provides affirmative evidence for the bridge-representation transferability across source-target types. In Figure 3(a), we report results on a select set of patching experiments: on *both* tasks with and without overlap in source and target types, we observe that a sparse set of attention heads consistently exhibits very strong *causal* effects in pushing the model’s “belief” from  $T_n^{(norm)}$  towards  $\hat{T}_n^{(alt)}$ ; the head group (24,30;31) is especially dominant.<sup>4</sup> To further understand whether intervening on (24,30;31) during the normal run really boosts the type-corrected alternative answer  $\hat{T}_n^{(alt)}$  (instead of only decreasing model’s confidence on the normal answer  $T_n^{(norm)}$ , which logit difference might not tell), in Figure 3(b), we show an example patching experiment result of [University, Code]→[City, Capital]. Surprisingly, at least 73% of the time, patching this single head group can boost the model’s rank of the alternative prompt’s answer into top 10 (and directly become the top-1 answer more than 40% of the time!), when its original rank, obtained on the normal prompt without intervention, is typically in the hundreds to thousands. In consideration of limited space, we visualize the full set of reciprocal rank and logit-difference variation results in Appendix A.2.

Finally, to understand the nature of (24,30;31)’s output embeddings better, in Figure 3(c), we visualize an example cosine similarity matrix of this attention head, with either “Italy” or “Spain” as the bridge values for  $S_n$  (the query source entity) in the prompts, across a total of 12 different combinations of bridge, source and target types. Specifically, for each combination of the bridge and source-target

<sup>4</sup>In our CMA experiments, we account for grouped-query attention by patching heads in groups of 2 on Gemma-2-27B. We noticed that this tends to produce stronger causal effects than with individual heads.

type shown in the grid, we sample 10 prompts which obey such requirement<sup>5</sup>, giving us a total of 120 prompts. We then obtain head group (24,30;31)’s embedding of these prompts at the last token position, and compute the pairwise cosine similarities. Observe that the embedding consistently exhibits strong *disentanglement* with respect to the bridge value in the prompt, *regardless of source and target types*. We shall provide more nuanced statistics of disentanglement strength in the next sub-section, when we discuss its relation with the number of ICL examples.

**Step 2: output-concept attention heads.** To support the hypothesis that the LLM refines the bridge value via certain output-concept representations, we need to perform CMA on normal-alternative prompt pairs which differ only in output type, and examine their disentanglement strength with respect to the output type. In particular, to construct an altered prompt, we keep everything in it the same as the normal demonstrations, besides the output type: for instance, if the normal output type is Capital, then the altered output type is Calling Code. This helps us isolate components which are *sensitive to the output concept, without surfacing components which are bridge-value dependent*. Due to space limitations, we delay the full CMA results to the appendix. Instead, we visualize the cosine similarity matrix of a select set of high-scoring heads, shown in Figure 4. In addition to measuring cosine similarity on our multi-hop prompts with Capital or Calling Code type output, we also design *negative-control* prompts, where we randomly shuffle the output. This leaves the prompts without structure, except asking for the model to output tokens belonging to either the “Capital” or “Calling Code” concept. We note that, as long as the output concept agrees, there is high similarity of these heads’ embeddings on the multi-hop and out-concept-only prompts.

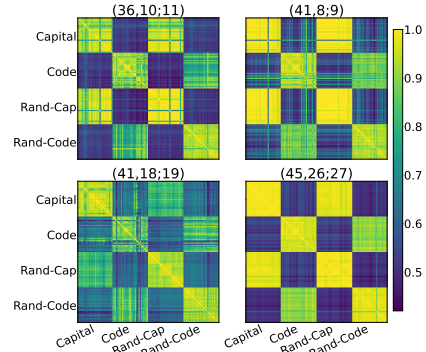


Figure 4: Cosine similarity maps of select “output-concept” heads, the majority of which are in the deeper layers.

### 2.3 Multi-hop circuit formation and the number of in-context examples

This sub-section focuses on illustrating the relation between the number of in-context examples versus (1) how strong a role the multi-hop mechanism plays in the LLM’s inference (via causal interventions), (2) disentanglement strength of key bridge-resolving attention heads. As we will show below, there is a general positive correlation between the number of shots and the two factors.

**More demonstrations  $\implies$  stronger causal score.** Figure 5 visualizes the experimental results. From Figure 5(a) and (b) and sub-figures, we observe a correlation between the number of shots (ICL examples) and the bridge-resolving heads’ “causal importance” in the model’s inference. When the number of shots is low, we find that they tend to exhibit weak causal influence on the model’s inference. For instance, as (b)(i) shows, at 2 shots, the 30<sup>th</sup> percentile of the alternative answer’s rank *after* patching at (24,30;31) is on the order of  $10^3$ . This is in stark contrast to how strong this head group’s causal influence is at 20 shots as we saw before.

**More demonstrations  $\implies$  stronger disentanglement, with a catch.** In Figure 5(c)(i) to (iv), we observe that the intra-bridge cosine similarity tends to cluster better as the number of shots increase, while the inter-bridge cosine similarities decay toward 0.2, with the two distributions overlapping less and less. Interestingly, the bridge-disentanglement strength is still non-trivial with very few shots, mirroring the causal-intervention results: regardless of how disentangled the representations are in the very-few-shot regime, the LLM does not “realize” how it should utilize the multi-hop sub-circuit.

### 2.4 Additional insights

We highlight a few additional mechanistic insights which are detailed in Appendix A.2 and A.3.

**Larger model size benefits concept disentanglement and utilization.** We experiment with a smaller variant of the Gemma 2 models, namely Gemma-2-2B. We find that its accuracies on these problems are significantly lower. Intriguingly, performing similar causal intervention experiments (as we did for the 27B) reveals that, *the 2B model has a weak and noisy version of the 27B’s bridge resolving*

<sup>5</sup>We only specify the bridge entity for  $S_n$  in the prompt; the bridge for  $S_i$  for all  $i < n$  are randomly chosen.

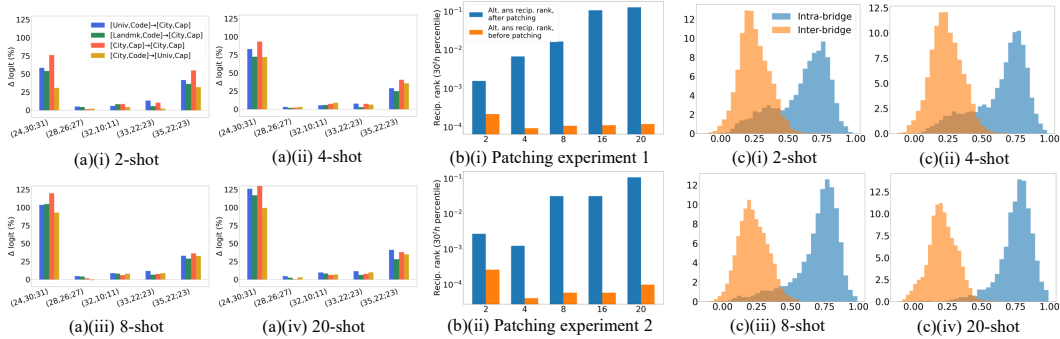


Figure 5: This figure illustrates how the transferability and disentanglement of the bridge representation increases as we increase the number of in-context examples. Figure series (a) and (b) present the transferability result, obtained by performing cross-problem-type patching, and measuring the causal influence of the patched representation. In (a)(i) to (iv), we plot the percentage logit variation of the attention heads found to output “bridge” values, measured on several intervention experiments. For (b)(i) and (ii), we zoom in on head group (24,30;31), and show its causal effects on two patching experiments, [University, Calling Code]→[City, Capital] and [Landmark, Calling Code]→[City, Capital]. The x-axis is the number of in-context examples, and the y-axis is the 30<sup>th</sup> percentile of the reciprocal rank of the alternative prompt’s answer. For (c)(i) to (iv), we plot the histogram of the disentanglement strength of the representations of head group (24,30;31), with the y-axis in percentage, and x-axis being cosine similarity.

*mechanism*. In particular, there also is a sparse set of attention heads which causally implicate the answer at a nontrivial degree when we intervene across source-target types, and exhibit noticeable disentanglement with respect to the bridge — they are just much weaker in strength compared to the 27B model. This suggests that increasing model size likely benefits latent concept disentanglement and effective utilization of such concept representations in the LLM. We detail this in Appendix A.2, and Figure 28.

**MLP functional role.** We find the MLPs having weaker causal scores than the attention heads at the last token position. The ones with nontrivial scores are in the layers after the bridge-resolving attention heads (24,30;31), and observed to primarily disentangle with respect to the output type — they do *not* participate heavily in resolving the bridge concept. This is presented in Figure 27 in Appendix A.2.

**The Company Problems, another set of two-hop ICL puzzles.** To complement our study on the Geography puzzles, we experiment with a similar, albeit smaller-scaled Company dataset in Appendix A.3. We collect information about well-known companies in the world, and construct problems [Product, Founder], [Founder, Product], [Product, Headquarter City], and [Founder, Headquarter City]: they all set the company name as the bridge value. We find that while the model’s accuracy on these problems are lower than that on the Geography puzzles by a nontrivial margin, we still observe causal and correlational evidence that the bridge-resolving mechanism is present in the model.

### 3 Disentanglement for Latent Continuous Parameterization

In this section, we consider two problems with numerical or continuous parameterization. For these experiments we study a very small transformer, with a similar architecture to GPT-2 [12]. We use a 2-layer 1-head transformer, with embedding dimension 128, trained with the AdamW optimizer. Additional details about training and hyperparameter choices are in the Appendix.

**add- $k$  Problem.** Each task is a sequence consisting of pairwise examples  $\{(x_i, y_i)\}_{i=1}^{n+1}$ , where  $y_i = x_i + k$ , for a given offset  $k$ . Here, we use integer inputs and offsets; all values are in  $\{0, \dots, V - 1\}$ , each treated as a distinct token. We consider a collection of  $K$  tasks parameterized by different offset values in  $\{k_i\}_{i=1}^K$ , where  $k_1 = 1$  and we fix  $k_{i+1} - k_i = 3$ . The model is trained autoregressively to predict the label for each example in the sequence. At test time, the model observes the first  $n$  examples and should predict  $y_{n+1} = x_{n+1} + k$  for the last example.

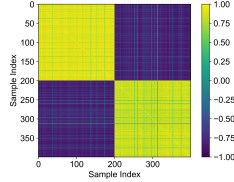


Figure 7: Cosine similarities between the layer-2 attention embeddings for 200 input sequences from two tasks/offsets for the *add-k* problem. Strong clustering between intra-task embeddings shows that the model disentangles the concept of different offsets.

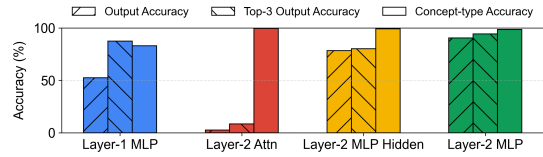


Figure 8: Results for linear probing the embeddings of the trained model at various locations to predict the final output and the task type for the *add-k* problem. The task type becomes disentangled at layer-2 attention, and the output is computed in layer-2 MLP.

**Circular-Trajectory Problem.** Here a task consists of a sequence  $\{\mathbf{x}_i\}_{i=1}^{n+1}$  of points on a circle centered at the origin. Each task is parameterized by the circle’s radius  $r$ ; for  $K$  tasks, the set of radii  $\{r_i\}_{i=1}^K$  is sampled uniformly from  $[1, 4]$ . A task sequence is generated as follows. We first sample  $\theta_0$  uniformly at random in  $[0, \frac{\pi}{2}]$ , so  $\mathbf{x}_1 = r[\cos \theta_0, \sin \theta_0]^T$ . Then, we select the *period*  $p$  randomly from  $\{2, 3, 4\}$ , which determines the number of equal consecutive step-sizes. Specifically, we first sample a sequence of  $\lfloor \frac{n}{p} \rfloor + 1$  unique step-sizes uniformly between  $[0, 1]$ , and then get the full sequence of steps  $\{a_i\}_{i=1}^n$ , where  $a_j = a_{j+1} = \dots = a_{j+p-1}$  for  $j \in \{0, p, 2p, \dots\}$ . Here, context length  $n = 12m + 1$  for integer  $m$ . We also sample  $c \in \{\pm 1\}$ , which denotes if the trajectory is clockwise or counterclockwise. Next, we generate a sequence of angles  $\{\theta_i\}_{i=1}^n$ , where  $\theta_i = \theta_0 + c \frac{2\pi}{n} \sum_{j \leq i} a_j$ . Using the sequence of angles, we generate the sequence,  $\mathbf{x}_{i+1} = rR(\theta_i)\mathbf{x}_i$ , where  $R(\theta)$  is the 2D rotation matrix for  $\theta$ . Fig. 6 shows an example. As in the previous problem, we train the transformer autoregressively on these types of sequences.

Additionally, in Appendix B, we consider another shape problem, namely the Rectangular-Trajectory problem, where the trajectories contain points on lying on axis-aligned rectangles centered at the origin. See Appendix B for a formal description. The Circular-Trajectory problem is parameterized by one continuous parameter (radius), whereas the Rectangular-Trajectory problem is parameterized by two parameters, namely the lengths of the two sides of the rectangle.

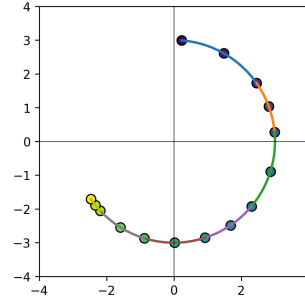


Figure 6: Illustration of an input sequence for the circle trajectory problem. Here, radius  $r = 3$ , period  $p = 2$ , sequence length  $n = 13$ . Every  $p$  consecutive steps on the trajectory are equal. We first sample  $\lfloor \frac{n}{p} \rfloor + 1$  unique step-sizes in  $[0, 1]$ , and get the full sequence  $\{a_1, a_2, a_3, a_4, \dots\}$ , where same colors denote equal step-sizes. Then, we generate the trajectory by rotating point  $\mathbf{x}_i$  clockwise by angle  $a_i \cdot \frac{2\pi}{n}$  (see text for formal description).

### 3.1 Results

**Existence of Task Vectors.** We first outline the process to identify the task vectors for the *add-k* problem. We set  $V = 100$ ,  $n = 4$ , and  $K = 2$ . Fig. 7 shows the cosine similarities between the layer-2 attention embeddings at the last position for 200 input sequences from each of the two tasks. We observe strong clustering between intra-task embeddings. This shows that the model disentangles the concept of different offset values in its representation.

To provide causal evidence for disentanglement, and to locate where the task vectors emerge in the model, we linear probe the embeddings of the trained model at various locations to predict the final output and the offset/task type. We probe embeddings from the output of the MLP at the first layer, the attention block at the second layer, and the hidden and output layers of the MLP at the second layer. The results are shown in Fig. 8. We observe that task type becomes disentangled at layer-2 attention, and the output is computed at layer-2 MLP. For each task, we treat the layer-2 attention embeddings averaged across 200 input sequences from that task as the task vector.

**Geometry of Task Vectors.** We analyze the geometry of the task vectors for the two problems. We visualize the task vectors by performing PCA and projecting them onto the first two principal components.

Fig. 9 presents the 2D PCA projection of the task vectors for the *add-k* problem, for  $K = 4, 8, 16$  tasks/offsets. We observe that in all three settings, the task vectors lie on a 1D linear manifold. In each of the three cases, more than 99.9% of the variance is explained by the first PC. Notably, the model compresses the concept of offsets into a line with the ordering of the offsets (lower to higher) preserved on the manifold (left to right).

To corroborate these results, we study the effect of steering using the task vectors. Specifically, let  $\mathbf{t}_1$  and  $\mathbf{t}_K$  denote the task vectors for offsets  $k_1$  and  $k_K$ , respectively. Then, for offset  $k_1$  ( $k_K$ ), we consider steering with  $(1 - \beta)\mathbf{t}_1 + \beta\mathbf{t}_K$  ( $(1 - \beta)\mathbf{t}_K + \beta\mathbf{t}_1$ ) and evaluate the accuracy for predicting the output based on the original offset  $k_1$  ( $k_K$ ), the ‘opposite’ offset  $k_K$  ( $k_1$ ), or the target offset  $(1 - \beta)k_1 + \beta k_K$  ( $(1 - \beta)k_K + \beta k_1$ ), where  $\beta \in [0, 1]$ . We consider the first and last offsets so that we can interpolate them to steer towards intermediate offsets. Fig. 10 presents the top-1 and top-3 accuracies for each case. High top-1 accuracies and  $\approx 100\%$  top-3 accuracies for the target for all considered values of  $\beta$  indicate that the model output is steered toward the target. This shows that interpolating along the top principal direction is successful at interpolating values of  $k$  in the task space, showing that the model is somewhat strikingly successful at capturing the latent concept.

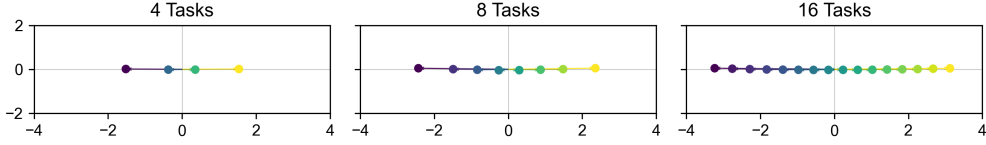


Figure 9: 2D PCA projection of the task vectors for the *add-k* problem. The task vectors lie on a 1D linear manifold. Here the number of tasks refers to the number of values of  $k$ .

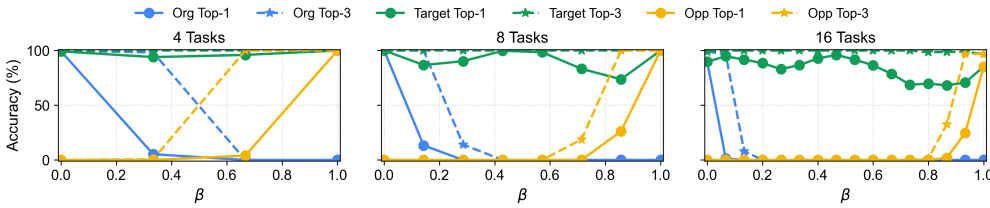


Figure 10: Steering with the task vectors for tasks  $k_1$  and  $k_K$  for the *add-k* problem (see text for details). We plot the top-1 and top-3 accuracies for predicting the output based on the original offset  $k_1$  ( $k_K$ ), the ‘opposite’ offset  $k_K$  ( $k_1$ ), or the target offset  $(1 - \beta)k_1 + \beta k_K$  ( $(1 - \beta)k_K + \beta k_1$ ), where  $\beta \in [0, 1]$ . The result shows that the model output can be steered toward the target.

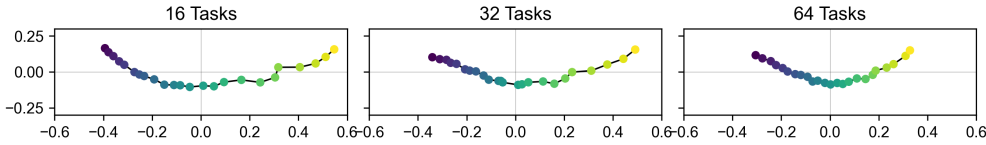


Figure 11: 2D PCA projection of the task vectors for the Circular-Trajectory problem. The task vectors lie on a smooth low-dimensional manifold. Here the number of tasks refers to the number of radius values used for training.

Fig. 11 presents the 2D PCA projection of the task vectors for the Circular-Trajectory problem, for  $K = 16, 32, 64$  (training) tasks/radii. In this setting, we consider  $K = 24$  radii, spaced evenly between  $[1, 4]$  to visualize the task vectors, since this task is continuous. We observe that in all three settings, the task vectors lie on a low-dimensional manifold. The variance explained by the first two PCs in the three cases is 97.05%, 96.44%, 93.68%, respectively. Similar to the previous setting, the order of the radii (lower to higher) is preserved in the compressed representation.

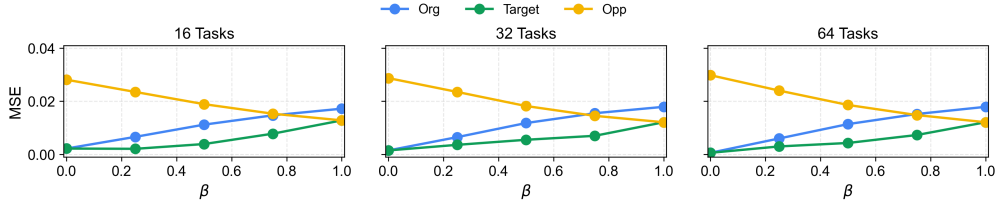


Figure 12: Steering with the task vectors for tasks  $r_1$  and  $r_K$  for the Circular-Trajectory problem (see text for details). The MSE between the radius inferred from the model output and the original radius  $r_1$  ( $r_K$ ), the ‘opposite’ radius  $r_K$  ( $r_1$ ), or the target radius  $(1 - \beta)r_1 + \beta r_K$  ( $(1 - \beta)r_K + \beta r_1$ ), where  $\beta \in [0, 1]$ , indicates that the model output can be steered toward the target.

Fig. 12 presents the results for steering the model output using the task vectors for radii  $r_1$  and  $r_K$ . We follow the same procedure as in the add- $k$  problem, with a different evaluation metric. We compute the norm of the generated output after steering as the model’s radius (since the center of the circles is fixed at the origin), and consider the MSE between these radii and the original radius  $r_1$  ( $r_K$ ), the ‘opposite’ radius  $r_K$  ( $r_1$ ), or the target radius  $(1 - \beta)r_1 + \beta r_K$  ( $(1 - \beta)r_K + \beta r_1$ ), where  $\beta \in [0, 1]$ , averaged over 200 sequences from each task. We observe that the MSE with the target radius is the lowest, which indicated the task vector can steer the model’s output toward the target.

In Appendix B, we examine the geometry of the task vectors for the Rectangular-Trajectory problem and find that the first 2 PCs lie on a two-dimensional manifold in that case as well.

## 4 Related Work

**In-context Learning Interpretation.** ICL abilities of transformer-based models were first observed by Brown et al. [1], which sparked work in analyzing this ability. This includes analyzing how pretrained LLMs solve ICL tasks requiring abilities such as copying, single-step reasoning, basic linguistics [4, 13, 14, 3, 2, 5], and smaller models trained on synthetic tasks like regression [15, 16, 17, 18, 19], discrete tasks [20], and mixture of Markov chains [21, 22, 23]. These setups enable discovery of relations between in-context and in-weight learning [24, 25, 26], and internal algorithms that models implement [4, 21, 23, 5]. We contribute to this line of work, by shedding light on how transformers solve ICL problems which have more intricate latent structures.

**Linear Representation Hypothesis (LRH).** Our results are also connected to the LRH, which essentially speculates that LLMs represent high-level concepts in (almost) linear latent directions [27, 28, 29, 30, 31, 32, 33, 34]. Many papers motivated by the LRH then find “concept” vectors that can capture directions of truthfulness [35, 36], sentiment [37], humor [38], toxicity [39], etc. We deepen this study, asking how LLMs’ representations capture/disentangle latent input concepts, and compose them during inference. In addition, the LRH is rooted in the field of mechanistic interpretability, which aims to reverse engineer mechanisms in transformer-based LMs [40, 4, 25, 41, 42, 43, 44, 45, 46, 47, 48, 49, 50].

**Task and Function Vectors.** A specific line of work in analyzing ICL mechanisms focus on task or function vectors. They essentially show that there exist certain causal patterns which capture the input-output relationship of the ICL task, on relatively simple problems such as “Country to Capital”, “Antonyms”, “Capitalize a Word” [2, 3, 6, 51]. Similarly, [52, 28, 53, 54] observed that LLMs tend to compress certain task or context information into sparse sets of vectors. We work with ICL problems with more complex latent structures, and our focus is not solely on (high-level) task vectors, but more on how the model disentangle and manipulate latent concepts useful to answering the query.

In addition, our work also complements the function vector analysis from contemporaneous work [7], providing add- $k$  results for smaller models where we have full control over training and can hence conclude that the geometry of the task vector only arises from the latent task structure. We also compare results from add- $k$  with other ICL tasks, giving additional insights.

## 5 Discussion and Conclusion

We showed that transformer-based models latently *disentangle* core concepts in the provided in-context examples, and *manipulate* them well. For 2-hop tasks, we found that models contain sparse

sets of attention heads responsible for first inferring the bridge entity and then resolving the output. For tasks with a continuous parameterization, we found that the model uses task vectors which closely capture the underlying parameterization. It would be interesting to understand the extent of this disentanglement across more diverse ICL tasks with various types of latent structures. It would also be very interesting to use latent concept identification to predict and improve ICL performance, and more efficiently learn new tasks which involve combining identified concepts.

## Acknowledgments

This work was supported in part by NSF CAREER Award CCF-2239265. The authors acknowledge the use of USC CARC’s Discovery cluster.

## References

- [1] Tom Brown, Benjamin Mann, Nick Ryder, Melanie Subbiah, Jared D Kaplan, Prafulla Dhariwal, Arvind Neelakantan, Pranav Shyam, Girish Sastry, Amanda Askell, Sandhini Agarwal, Ariel Herbert-Voss, Gretchen Krueger, Tom Henighan, Rewon Child, Aditya Ramesh, Daniel Ziegler, Jeffrey Wu, Clemens Winter, Chris Hesse, Mark Chen, Eric Sigler, Mateusz Litwin, Scott Gray, Benjamin Chess, Jack Clark, Christopher Berner, Sam McCandlish, Alec Radford, Ilya Sutskever, and Dario Amodei. Language models are few-shot learners. In H. Larochelle, M. Ranzato, R. Hadsell, M.F. Balcan, and H. Lin, editors, *Advances in Neural Information Processing Systems*, volume 33, pages 1877–1901. Curran Associates, Inc., 2020. URL [https://proceedings.neurips.cc/paper\\_files/paper/2020/file/1457c0d6bfc4967418bfb8ac142f64a-Paper.pdf](https://proceedings.neurips.cc/paper_files/paper/2020/file/1457c0d6bfc4967418bfb8ac142f64a-Paper.pdf).
- [2] Eric Todd, Millicent Li, Arnab Sen Sharma, Aaron Mueller, Byron C Wallace, and David Bau. Function vectors in large language models. In *The Twelfth International Conference on Learning Representations*, 2024. URL <https://openreview.net/forum?id=AwxytyMwaG>.
- [3] Roei Hendel, Mor Geva, and Amir Globerson. In-context learning creates task vectors. In *The 2023 Conference on Empirical Methods in Natural Language Processing*, 2023. URL <https://openreview.net/forum?id=QYvFULF19n>.
- [4] Catherine Olsson, Nelson Elhage, Neel Nanda, Nicholas Joseph, Nova DasSarma, Tom Henighan, Ben Mann, Amanda Askell, Yuntao Bai, Anna Chen, Tom Conerly, Dawn Drain, Deep Ganguli, Zac Hatfield-Dodds, Danny Hernandez, Scott Johnston, Andy Jones, Jackson Kernion, Liane Lovitt, Kamal Ndousse, Dario Amodei, Tom Brown, Jack Clark, Jared Kaplan, Sam McCandlish, and Chris Olah. In-context learning and induction heads. *Transformer Circuits Thread*, 2022. <https://transformer-circuits.pub/2022/in-context-learning-and-induction-heads/index.html>.
- [5] Kayo Yin and Jacob Steinhardt. Which attention heads matter for in-context learning? *arXiv preprint arXiv:2502.14010*, 2025.
- [6] Guy Davidson, Todd M. Gureckis, Brenden M. Lake, and Adina Williams. Do different prompting methods yield a common task representation in language models?, 2025. URL <https://arxiv.org/abs/2505.12075>.
- [7] Xinyan Hu, Kayo Yin, Michael I Jordan, Jacob Steinhardt, and Lijie Chen. Understanding in-context learning of addition via activation subspaces. *arXiv preprint arXiv:2505.05145*, 2025.
- [8] Gemma Team. Gemma 2: Improving open language models at a practical size, 2024. URL <https://arxiv.org/abs/2408.00118>.
- [9] Sohee Yang, Elena Gribovskaya, Nora Kassner, Mor Geva, and Sebastian Riedel. Do large language models latently perform multi-hop reasoning? In *Proceedings of the 62nd Annual Meeting of the Association for Computational Linguistics (Volume 1: Long Papers)*, pages 10210–10229, 2024.

- [10] Judea Pearl. *Direct and Indirect Effects*, page 373–392. Association for Computing Machinery, New York, NY, USA, 1 edition, 2022. ISBN 9781450395861. URL <https://doi.org/10.1145/3501714.3501736>.
- [11] Fred Zhang and Neel Nanda. Towards best practices of activation patching in language models: Metrics and methods. In *The Twelfth International Conference on Learning Representations*, 2024. URL <https://openreview.net/forum?id=Hf17y6u9BC>.
- [12] Alec Radford, Jeff Wu, Rewon Child, David Luan, Dario Amodei, and Ilya Sutskever. Language models are unsupervised multitask learners. In *OpenAI blog*, 2019. URL <https://api.semanticscholar.org/CorpusID:160025533>.
- [13] Sewon Min, Xinxi Lyu, Ari Holtzman, Mikel Artetxe, Mike Lewis, Hannaneh Hajishirzi, and Luke Zettlemoyer. Rethinking the role of demonstrations: What makes in-context learning work? In Yoav Goldberg, Zornitsa Kozareva, and Yue Zhang, editors, *Proceedings of the 2022 Conference on Empirical Methods in Natural Language Processing*, pages 11048–11064, Abu Dhabi, United Arab Emirates, December 2022. Association for Computational Linguistics. doi: 10.18653/v1/2022.emnlp-main.759. URL <https://aclanthology.org/2022.emnlp-main.759/>.
- [14] Denny Zhou, Nathanael Schärli, Le Hou, Jason Wei, Nathan Scales, Xuezhi Wang, Dale Schuurmans, Claire Cui, Olivier Bousquet, Quoc Le, and Ed Chi. Least-to-most prompting enables complex reasoning in large language models, 2023. URL <https://arxiv.org/abs/2205.10625>.
- [15] Shivam Garg, Dimitris Tsipras, Percy Liang, and Gregory Valiant. What can transformers learn in-context? a case study of simple function classes. In Alice H. Oh, Alekh Agarwal, Danielle Belgrave, and Kyunghyun Cho, editors, *Advances in Neural Information Processing Systems*, 2022. URL <https://openreview.net/forum?id=f1NZJ2e0et>.
- [16] Johannes Von Oswald, Eyvind Niklasson, Ettore Randazzo, Joao Sacramento, Alexander Mordvintsev, Andrey Zhmoginov, and Max Vladymyrov. Transformers learn in-context by gradient descent. In Andreas Krause, Emma Brunskill, Kyunghyun Cho, Barbara Engelhardt, Sivan Sabato, and Jonathan Scarlett, editors, *Proceedings of the 40th International Conference on Machine Learning*, volume 202 of *Proceedings of Machine Learning Research*, pages 35151–35174. PMLR, 23–29 Jul 2023. URL <https://proceedings.mlr.press/v202/von-oswald23a.html>.
- [17] Ekin Akyürek, Dale Schuurmans, Jacob Andreas, Tengyu Ma, and Denny Zhou. What learning algorithm is in-context learning? Investigations with linear models. In *Int. Conference on Learning Representations*, 2023. URL <https://openreview.net/forum?id=0g0X4H8yN4I>.
- [18] Yu Bai, Fan Chen, Huan Wang, Caiming Xiong, and Song Mei. Transformers as statisticians: Provable in-context learning with in-context algorithm selection, 2023. URL <https://arxiv.org/abs/2306.04637>.
- [19] Tianyu Guo, Hanlin Zhu, Ruiqi Zhang, Jiantao Jiao, Song Mei, Michael I Jordan, and Stuart Russell. How do llms perform two-hop reasoning in context? *arXiv preprint arXiv:2502.13913*, 2025.
- [20] Satwik Bhattamishra, Arkil Patel, Phil Blunsom, and Varun Kanade. Understanding in-context learning in transformers and LLMs by learning to learn discrete functions. In *The Twelfth International Conference on Learning Representations*, 2024. URL <https://openreview.net/forum?id=ekeyCgeRfC>.
- [21] Ezra Edelman, Nikolaos Tsilivis, Benjamin L. Edelman, Eran Malach, and Surbhi Goel. The evolution of statistical induction heads: In-context learning markov chains. In *The Thirty-eighth Annual Conference on Neural Information Processing Systems*, 2024. URL <https://openreview.net/forum?id=qaRT6QTIqJ>.
- [22] Nived Rajaraman, Marco Bondaschi, Ashok Vardhan Makkuva, Kannan Ramchandran, and Michael Gastpar. Transformers on markov data: Constant depth suffices. In *The Thirty-eighth Annual Conference on Neural Information Processing Systems*, 2024. URL <https://openreview.net/forum?id=5uG9tp3v2q>.

- [23] Core Francisco Park, Ekdeep Singh Lubana, and Hidenori Tanaka. Competition dynamics shape algorithmic phases of in-context learning. In *The Thirteenth International Conference on Learning Representations*, 2025. URL <https://openreview.net/forum?id=XgH1wfHSX8>.
- [24] Ziqian Lin and Kangwook Lee. Dual operating modes of in-context learning. In *Proceedings of the 41st International Conference on Machine Learning, ICML'24*. JMLR.org, 2024.
- [25] Aaditya K. Singh, Ted Moskowitz, Sara Dragutinovic, Felix Hill, Stephanie C. Y. Chan, and Andrew M. Saxe. Strategy cooperation explains the emergence and transience of in-context learning, 2025. URL <https://arxiv.org/abs/2503.05631>.
- [26] Jacob Russin, Ellie Pavlick, and Michael J. Frank. The dynamic interplay between in-context and in-weight learning in humans and neural networks, 2025. URL <https://arxiv.org/abs/2402.08674>.
- [27] Kiho Park, Yo Joong Choe, and Victor Veitch. The linear representation hypothesis and the geometry of large language models. In *International Conference on Machine Learning*, pages 39643–39666. PMLR, 2024.
- [28] Jack Merullo, Carsten Eickhoff, and Ellie Pavlick. Language models implement simple Word2Vec-style vector arithmetic. In Kevin Duh, Helena Gomez, and Steven Bethard, editors, *Proceedings of the 2024 Conference of the North American Chapter of the Association for Computational Linguistics: Human Language Technologies (Volume 1: Long Papers)*, pages 5030–5047, Mexico City, Mexico, June 2024. Association for Computational Linguistics. doi: 10.18653/v1/2024.naacl-long.281. URL <https://aclanthology.org/2024.naacl-long.281/>.
- [29] Kiho Park, Yo Joong Choe, Yibo Jiang, and Victor Veitch. The geometry of categorical and hierarchical concepts in large language models, 2025. URL <https://arxiv.org/abs/2406.01506>.
- [30] Minyoung Huh, Brian Cheung, Tongzhou Wang, and Phillip Isola. The platonic representation hypothesis. *arXiv preprint arXiv:2405.07987*, 2024.
- [31] Gabriel Ilharco, Marco Tulio Ribeiro, Mitchell Wortsman, Suchin Gururangan, Ludwig Schmidt, Hannaneh Hajishirzi, and Ali Farhadi. Editing models with task arithmetic, 2023. URL <https://arxiv.org/abs/2212.04089>.
- [32] Yuxiao Li, Eric J. Michaud, David D. Baek, Joshua Engels, Xiaoqing Sun, and Max Tegmark. The geometry of concepts: Sparse autoencoder feature structure. *Entropy*, 27(4), 2025. ISSN 1099-4300. doi: 10.3390/e27040344. URL <https://www.mdpi.com/1099-4300/27/4/344>.
- [33] Clément Dumas, Chris Wendler, Veniamin Veselovsky, Giovanni Monea, and Robert West. Separating tongue from thought: Activation patching reveals language-agnostic concept representations in transformers, 2025. URL <https://arxiv.org/abs/2411.08745>.
- [34] Daniel Beaglehole, Adityanarayanan Radhakrishnan, Enric Boix-Adserà, and Mikhail Belkin. Aggregate and conquer: detecting and steering llm concepts by combining nonlinear predictors over multiple layers, 2025. URL <https://arxiv.org/abs/2502.03708>.
- [35] Samuel Marks and Max Tegmark. The geometry of truth: Emergent linear structure in large language model representations of true/false datasets, 2024. URL <https://arxiv.org/abs/2310.06824>.
- [36] Andy Arditi, Oscar Obeso, Aquib Syed, Daniel Paleka, Nina Panickssery, Wes Gurnee, and Neel Nanda. Refusal in language models is mediated by a single direction, 2024. URL <https://arxiv.org/abs/2406.11717>.
- [37] Curt Tigges, Oskar John Hollinsworth, Neel Nanda, and Atticus Geiger. Language models linearly represent sentiment, 2024. URL <https://openreview.net/forum?id=iGDWZFc7Ya>.
- [38] Dimitri von Rütte, Sotiris Anagnostidis, Gregor Bachmann, and Thomas Hofmann. A language model’s guide through latent space, 2024. URL <https://arxiv.org/abs/2402.14433>.

- [39] Edward Turner, Anna Soligo, Mia Taylor, Senthoran Rajamanoharan, and Neel Nanda. Model organisms for emergent misalignment, 2025. URL <https://arxiv.org/abs/2506.11613>.
- [40] Nelson Elhage, Neel Nanda, Catherine Olsson, Tom Henighan, Nicholas Joseph, Ben Mann, Amanda Askell, Yuntao Bai, Anna Chen, Tom Conerly, Nova DasSarma, Dawn Drain, Deep Ganguli, Zac Hatfield-Dodds, Danny Hernandez, Andy Jones, Jackson Kernion, Liane Lovitt, Kamal Ndousse, Dario Amodei, Tom Brown, Jack Clark, Jared Kaplan, Sam McCandlish, and Chris Olah. A mathematical framework for transformer circuits. *Transformer Circuits Thread*, 2021. <https://transformer-circuits.pub/2021/framework/index.html>.
- [41] Zhengxuan Wu, Atticus Geiger, Thomas Icard, Christopher Potts, and Noah Goodman. Interpretability at scale: Identifying causal mechanisms in alpaca. In *Thirty-seventh Conference on Neural Information Processing Systems*, 2023. URL <https://openreview.net/forum?id=nRfClmMhVX>.
- [42] Kevin Ro Wang, Alexandre Variengien, Arthur Conmy, Buck Shlegeris, and Jacob Steinhardt. Interpretability in the wild: a circuit for indirect object identification in GPT-2 small. In *The Eleventh International Conference on Learning Representations*, 2023. URL <https://openreview.net/forum?id=NpsVSN6o4ul>.
- [43] Guan Zhe Hong, Nishanth Dikkala, Enming Luo, Cyrus Rashtchian, Xin Wang, and Rina Panigrahy. How transformers solve propositional logic problems: A mechanistic analysis. *arXiv preprint arXiv:2411.04105*, 2024.
- [44] Jannik Brinkmann, Abhay Sheshadri, Victor Levoso, Paul Swoboda, and Christian Bartelt. A mechanistic analysis of a transformer trained on a symbolic multi-step reasoning task. *arXiv preprint arXiv:2402.11917*, 2024.
- [45] Aleksandra Bakalova, Yana Veitsman, Xinting Huang, and Michael Hahn. Contextualize-then-aggregate: Circuits for in-context learning in gemma-2 2b. *arXiv preprint arXiv:2504.00132*, 2025.
- [46] Lovis Heindrich, Philip Torr, Fazl Barez, and Veronika Thost. Do sparse autoencoders generalize? a case study of answerability, 2025. URL <https://arxiv.org/abs/2502.19964>.
- [47] Badr AlKhamissi, Greta Tuckute, Antoine Bosselut, and Martin Schrimpf. The llm language network: A neuroscientific approach for identifying causally task-relevant units, 2025. URL <https://arxiv.org/abs/2411.02280>.
- [48] Jesse Vig, Sebastian Gehrmann, Yonatan Belinkov, Sharon Qian, Daniel Nevo, Yaron Singer, and Stuart Shieber. Investigating gender bias in language models using causal mediation analysis. In H. Larochelle, M. Ranzato, R. Hadsell, M.F. Balcan, and H. Lin, editors, *Advances in Neural Information Processing Systems*, volume 33, pages 12388–12401. Curran Associates, Inc., 2020. URL [https://proceedings.neurips.cc/paper\\_files/paper/2020/file/92650b2e92217715fe312e6fa7b90d82-Paper.pdf](https://proceedings.neurips.cc/paper_files/paper/2020/file/92650b2e92217715fe312e6fa7b90d82-Paper.pdf).
- [49] David D. Baek and Max Tegmark. Towards understanding distilled reasoning models: A representational approach, 2025. URL <https://arxiv.org/abs/2503.03730>.
- [50] Zijian Wang and Chang Xu. Functional abstraction of knowledge recall in large language models, 2025. URL <https://arxiv.org/abs/2504.14496>.
- [51] Kayo Yin and Jacob Steinhardt. Which attention heads matter for in-context learning?, 2025. URL <https://arxiv.org/abs/2502.14010>.
- [52] Sheng Liu, Haotian Ye, Lei Xing, and James Zou. In-context vectors: making in context learning more effective and controllable through latent space steering. In *Proceedings of the 41st International Conference on Machine Learning, ICML’24*. JMLR.org, 2024.
- [53] Zhuowei Li, Zihao Xu, Ligong Han, Yunhe Gao, Song Wen, Di Liu, Hao Wang, and Dimitris N. Metaxas. Implicit in-context learning. In *The Thirteenth International Conference on Learning Representations*, 2025. URL <https://openreview.net/forum?id=G7u4ue6ncT>.

- [54] Badr AlKhamissi, Greta Tuckute, Antoine Bosselut, and Martin Schrimpf. The LLM language network: A neuroscientific approach for identifying causally task-relevant units. In Luis Chiruzzo, Alan Ritter, and Lu Wang, editors, *Proceedings of the 2025 Conference of the Nations of the Americas Chapter of the Association for Computational Linguistics: Human Language Technologies (Volume 1: Long Papers)*, pages 10887–10911, Albuquerque, New Mexico, April 2025. Association for Computational Linguistics. ISBN 979-8-89176-189-6. doi: 10.18653/v1/2025.naacl-long.544. URL <https://aclanthology.org/2025.naacl-long.544/>.
- [55] Kevin Meng, David Bau, Alex J Andonian, and Yonatan Belinkov. Locating and editing factual associations in GPT. In Alice H. Oh, Alekh Agarwal, Danielle Belgrave, and Kyunghyun Cho, editors, *Advances in Neural Information Processing Systems*, 2022. URL <https://openreview.net/forum?id=-h6WAS6eE4>.
- [56] Tianyi Zhou, Deqing Fu, Vatsal Sharan, and Robin Jia. Pre-trained large language models use fourier features to compute addition. In *NeurIPS*, 2024.
- [57] Subhash Kantamneni and Max Tegmark. Language models use trigonometry to do addition. *arXiv preprint arXiv:2502.00873*, 2025.

## Appendix

<b>A Experimental Details and Additional Experiments for Section 2</b>	<b>17</b>
A.1 Details on experimental setup and techniques . . . . .	17
A.2 Additional details on experiments with the Geography 2-hop ICL puzzles . . . . .	19
A.3 The Company Puzzles, Another Multi-Hop ICL Task . . . . .	27
<b>B Experimental Details and Additional Experiments for Section 3</b>	<b>29</b>
B.1 More on the add- $k$ Problem . . . . .	29
B.2 More on the Circular-Trajectory Problem . . . . .	29
B.3 More on the Rectangular-Trajectory Problem . . . . .	30
<b>C Limitations and Broader Impact</b>	<b>30</b>

## A Experimental Details and Additional Experiments for Section 2

### A.1 Details on experimental setup and techniques

**Causal mediation analysis.** We primarily rely on causal mediation analysis (CMA), a.k.a. activation patching in the mechanistic interpretability literature, to obtain causal evidence for our claims in the LLM studies.

At a high level, CMA is about the study of indirect effects (IE) and direct effects (DE) in a system with causal relations [10]. Consider the following classical diagram of CMA, in Figure 13.

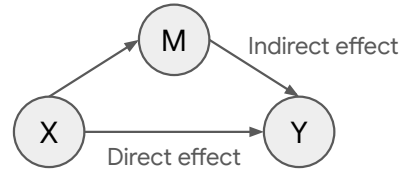


Figure 13: Basic illustration of CMA.  $X$  = input (exposure),  $M$  = mediator,  $Y$  = output (outcome).

Suppose we wish to understand whether a certain mediator  $M$  plays an important role in the causal path from the input  $X$  to the outcome  $Y$ . We decompose the “total effect” of  $X$  on  $Y$  into the sum of *direct* and *indirect* effects (DEs and IEs), as shown in the figure. The indirect effect measures how important a role the mediator  $M$  plays in the causal path  $X \rightarrow Y$ . To measure it, we compute  $Y$  given  $X$ , except that we artificially hold  $M$ ’s output to its “corrupted” version, which is obtained by computing  $M$  on a counterfactual (“corrupted”) version of the input. A significant change in  $Y$  indicates a strong IE, which implies that  $M$  is important in the causal path. On the other hand, a weak IE implies a strong DE, meaning that the mediator does not play a strong causal role in the system (for the distribution of inputs of interest).

There are two common classes of interventions in mechanistic interpretability for localizing model components with strong IE in the causal graph. The first class is simple ablation, such as mean ablation (replace activation of the mediator by its average output on a distribution of interest) [42] or “noising” [55]. While this type of intervention is easy to perform, it typically leads to poor localization, surfacing low-level processing components irrelevant to the study [11].

The other class, which we employ, is “interchange” intervention: it requires construction of alternative prompts which differ from the normal prompt in subtle ways, requiring careful consideration of the problem’s nature, but allows “causal surgery” which surfaces model components with specific functional roles. Technically speaking, we are measuring the *natural indirect effects* of the mediator. In particular, it works as follows. We first run the system (the LLM) on both normal and alternative (or sometimes called counterfactual) inputs, and cache the output of the mediator  $M$ . We then hold  $M$ ’s output to its alternative version, as we run the full system (the LLM) on the normal prompt. Everything downstream in the causal graph from  $M$  are also influenced, up to the output  $Y$ . This helps us measure how the mediator  $M$  causally implicate the answer. Or more intuitively, it measures how “flipping” the output of  $M$  causally influences the LLM’s “belief” in the alternative answer over the normal answer.

What makes our intervention experiments somewhat novel lies in exactly how we measure the IE. In particular, as we briefly discussed Section 2.1 and 2.2, we do *not* directly use the alternative prompt’s ground truth answer to measure how well we are “bending” the model’s “belief” through intervention. We discuss our method in greater detail here.

First, to understand whether certain attention heads have functional roles in processing the query source entity  $S_n$  which transcend source-target types of the two-hop problems, we work with normal-alternative prompts with distinct source and target types, such as sampling an *alternative* prompt “EPFL, 41. ... University of Tokyo, ” ([University, Code] problem), and a *normal* prompt “Okinawa, Tokyo. ... Chicago, ” ([City, Capital] problem). We hypothesize that there are certain model components which output the bridge concept, which is then composed with the target/output concept of the problem. For the normal example, this means “Chicago” $\rightarrow$ “USA” is resolved first, then the model executes Capital(USA) = Washington D.C. as the output. This means that, patching a model component’s activation from the alternative prompt onto its activation on a normal prompt, would cause the model to favor the answer of the alternative prompt, but with the same target semantic type as the normal prompt. In our running example, this would be “Tokyo”, the capital of “Japan”, the country (bridge) of the university “University of Tokyo”.

It follows that, to evaluate the “causal effects” of such a bridge-resolving component, we should set  $\hat{T}_n^{(alt)} = \text{Type}_{\text{norm}}(T_n^{(alt)})$ . We then measure the (expected) intervened logit difference

$$\Delta_{\text{alt}\rightarrow\text{norm}} = \mathbb{E} \left[ \text{logit}^{\text{alt}\rightarrow\text{norm}}(\mathbf{p}_{\text{norm}})[T_n^{(\text{norm})}] - \text{logit}^{\text{alt}\rightarrow\text{norm}}(\mathbf{p}_{\text{norm}})[\hat{T}_n^{(\text{alt})}] \right], \quad (4)$$

where  $\mathbf{p}_{\text{norm}} = [S_1^{(\text{norm})}, T_1^{(\text{norm})}, \dots, S_n^{(\text{norm})}]$  is the normal prompt,  $\text{logit}^{\text{alt}\rightarrow\text{norm}}(\mathbf{p}_{\text{norm}})$  indicates the logits of the model obtained after intervention while running the model on the normal prompt, and  $\text{logit}(\mathbf{p}_{\text{norm}})$  indicates the logits of the model running naturally (un-intervened) on the normal prompt. Moreover, when we measure the rank of the model’s answer when intervened, we also use  $\hat{T}_n^{(alt)}$  as the target.

*Remark.* To normalize our logit-difference variations, we compute

$$\bar{\Delta} = \frac{\Delta_{\text{norm}} - \Delta_{\text{alt}\rightarrow\text{norm}}}{\Delta_{\text{norm}}}, \quad (5)$$

where

$$\Delta_{\text{norm}} = \mathbb{E} \left[ \text{logit}(\mathbf{p}_{\text{norm}})[T_n^{(\text{norm})}] - \text{logit}(\mathbf{p}_{\text{norm}})[\hat{T}_n^{(\text{alt})}] \right]. \quad (6)$$

**Problem settings and overall observations.** We primarily work with the Geography and Company 2-hop ICL problems to, and with the LLM Gemma-2-27B. The former problem setting was described in the main text (with further elaboration in the Appendix later), while the latter will be introduced later, to add further generality to our study.

At a high level, in both the Geography and Company 2-hop ICL problems, we obtained causal and correlational evidence that highly localized groups of attention heads output the representation of the “bridge” concept based on the query, and the model later utilizes such representation to produce the output. Furthermore, an interesting technical observation is that multiplying the patched representation at these attention heads with a constant slightly above 1 (e.g. 1.5 to 4.0) tend to improve the intervention results. Finally, we make the observation that a smaller LLM, namely Gemma-2-2B, also possesses attention heads which have a nontrivial causal role in inferring the bridge representations. However, the representations are poorly disentangled, potentially leading to the model’s low accuracy on the ICL problems.

**Compute.** Our LLM experiments are conducted on 2 H200 GPUs, totaling around 160 hours of compute.

**Licenses.** We use the pretrained Gemma 2 models for our LLM experiments. They have the following license information.

- Models: Gemma-2-27B and Gemma-2-2B (google/gemma-2-27b and google/gemma-2-2B on Huggingface)
- License: Gemma Terms of Use (Google, 21 Feb 2024)
- Link: <https://ai.google.dev/gemma/terms>
- Notes: Commercial use permitted subject to Gemma Prohibited-Use Policy.

## A.2 Additional details on experiments with the Geography 2-hop ICL puzzles

**Dataset construction.** Our 2-hop ICL dataset is constructed by first prompting ChatGPT for the raw data, then clean and add to the data manually. The geography puzzles are cleaned to reduce leakage of source types, for instance, ChatGPT sometimes append city or state/province/region to a landmark, which we remove to ensure that the Landmark source type remains sufficiently distinct from the City source type. University names sometimes cannot avoid such overlap, e.g. University of California, Berkeley indeed has city name in it.

**Causal evidence.** Recall that in the main text, to provide causal evidence for the bridge-resolving mechanism, we primarily presented causal intervention experiments where we treated [City, Capital] as the problem type we intervene on, using cross-type prompts [University, Calling Code], [Landmark, Calling Code] to show causal evidence for the bridge-resolving heads. Here, we add further evidence by having other source-target types. The results are presented in Figures 14 to 23, indexed as follows:

1. Experiment [City, Capital]→[Landmark, Calling Code]: Figure 14
2. Experiment [University, Capital]→[Landmark, Calling Code]: Figure 15
3. Experiment [City, Capital]→[University, Calling Code]: Figure 16
4. Experiment [Landmark, Capital]→[University, Calling Code]: Figure 17
5. Experiment [University, Capital]→[City, Calling Code]: Figure 18
6. Experiment [Landmark, Capital]→[City, Calling Code]: Figure 19
7. Experiment [City, Calling Code]→[University, Capital]: Figure 20
8. Experiment [Landmark, Calling Code]→[University, Capital]: Figure 21
9. Experiment [City, Calling Code]→[Landmark, Capital]: Figure 22
10. Experiment [University, Calling Code]→[Landmark, Capital]: Figure 23

Every patching experiment is performed on at least 100 prompts. As we can see, the general trend is that there is strong transferability of the bridge representation across the problem types, including when the source and target types have no overlap, giving us causal evidence that head groups (24,30;31), (35,22;23) are “resolving the bridge”.

*Scaling constant for bridge intervention.* We found that for some of the transfer experiments, multiplying the patched representation for the heads (24,30;31), (35,22;23) improves the result, i.e. there is a greater percentage of samples where the alternative answer is boosted into the top-10 (or even top-1) answers of the model after intervention. Therefore, we also report those results. An intriguing property of this scaling constant is that it typically works best around 2.0. At 4.0, we

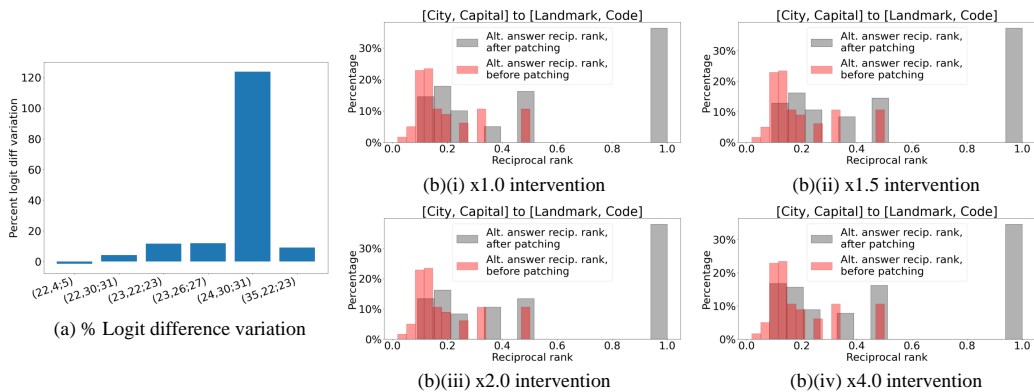


Figure 14: Gemma-2-27B [City, Capital]→[Landmark, Code] transfer experiments, intervening head groups (24, 30; 31), (35, 22; 23). We show the percentage logit-difference variation in (a), and reciprocal rank of the answer answer before and after intervention in the (b) series of figures, with different scaling constants in {1.0, 1.5, 2.0, 4.0}. We observe strong causal effects of the two attention head groups. Here, the scaling constant does not significantly affect the intervention performance.

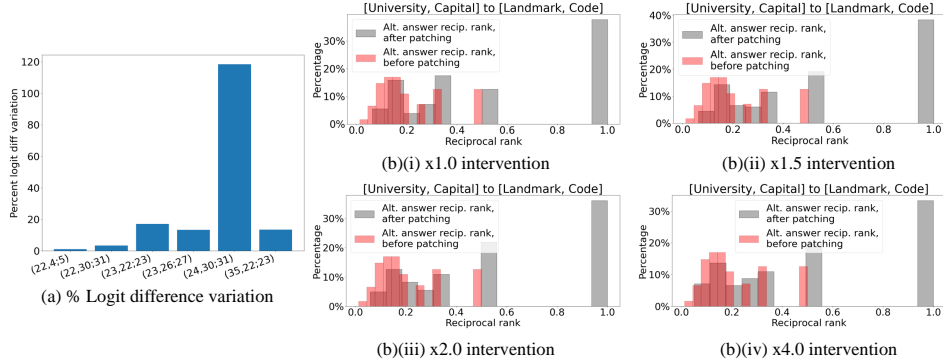


Figure 15: Gemma-2-27B [University, Capital]→[Landmark, Code] transfer experiments, intervening head groups (24, 30; 31), (35, 22; 23). We show the percentage logit-difference variation in (a), and reciprocal rank of the answer answer before and after intervention in the (b) series of figures, with different scaling constants in {1.0, 1.5, 2.0, 4.0}. We observe strong causal effects of the two head groups. Interesting, past a scaling constant of 1.5, we observe decline in intervention performance.

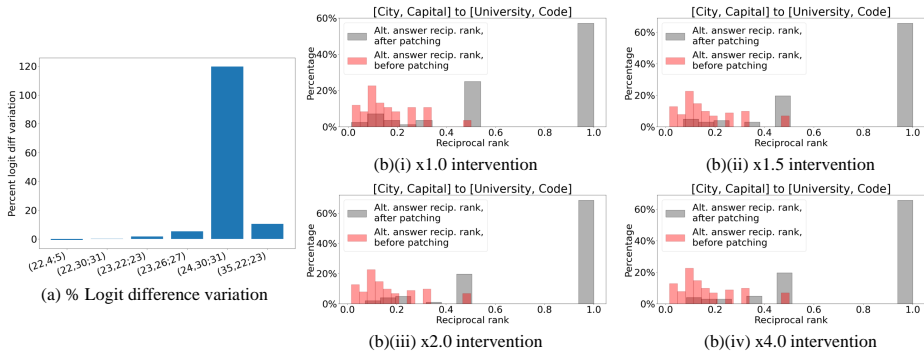


Figure 16: Gemma-2-27B [City, Capital]→[University, Code] transfer experiments, intervening head groups (24, 30; 31), (35, 22; 23). We show the percentage logit-difference variation in (a), and reciprocal rank of the answer answer before and after intervention in the (b) series of figures, with different scaling constants in {1.0, 1.5, 2.0, 4.0}. We observe strong causal effects of the two attention head groups, boosting the alternative answer into top 1 around 60% of the time! Additionally, the scaling constant does not significantly affect the intervention performance in this experiment.

often observe *saturation* or even *decline* in the intervened alternative answer’s rank, such as in the [University, Capital]→[City, Calling Code] experiment shown in Figure 18.

**The output-concept heads.** While the main interest of this work lies in the bridge-resolving mechanism enabled by the sparse set of attention heads discussed above, we also present more analysis of the output-concept heads, whose embedding tends to cluster with respect to the output concept (Capital versus Calling Code). To localize these heads, as discussed in our main text, we generate normal-alternative prompt pairs where we only change the target/output type of the normal prompt to generate the alternative prompt, but keep the  $S_i$ ’s to be identical across the prompt pairs for all  $i \leq n$ . This helps us surface components which are independent of the query and bridge value, and sensitive to the output/target type for the ICL problem. The results are shown in Figure 24 and 25, where we run the intervention experiment [Landmark, Calling Code]→[Landmark, Capital] (due to limitations in time and computing resources, we could not sweep all the source-target combinations as of this version of the paper). As we can see, these head groups with the strongest causal scores indeed tend to exhibit sensitivity to output type, and insensitivity to source/input type and query and bridge value. Moreover, they are more concentrated in the deeper layers of the model.

**Statistics of alternative-type answers.** A natural question to challenge the bridge-resolving mechanism is as follows. Say we are performing intervention by sampling alternative prompts from the problem type [University, Calling Code], and normal prompts from the type [City, Capital]: even

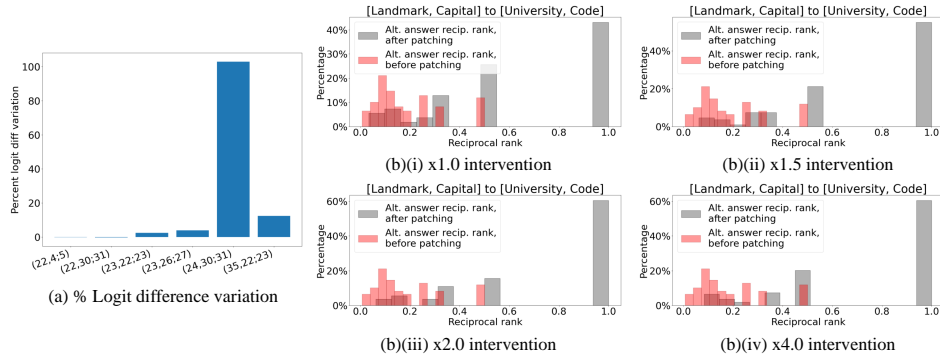


Figure 17: Gemma-2-27B [Landmark, Capital]→[University, Code] transfer experiments, intervening head groups (24, 30; 31), (35, 22; 23). We show the percentage logit-difference variation in (a), and reciprocal rank of the answer answer before and after intervention in the (b) series of figures, with different scaling constants in {1.0, 1.5, 2.0, 4.0}. We observe strong causal effects of the two attention head groups. Here, the positive effects of the scaling constant saturates around 2.0.

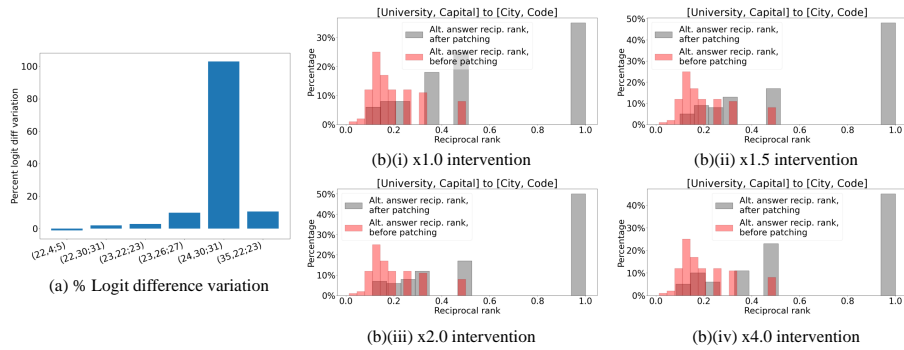


Figure 18: Gemma-2-27B [University, Capital]→[City, Code] transfer experiments, intervening head groups (24, 30; 31), (35, 22; 23). We show the percentage logit-difference variation in (a), and reciprocal rank of the answer answer before and after intervention in the (b) series of figures, with different scaling constants in {1.0, 1.5, 2.0, 4.0}. Interestingly, we observe decline in the intervention’s accuracy as we push the scaling constant from 2.0 to 4.0 (top-1 accuracy decreases from around 50% to slightly above 40%), indicating a subtle regime in which the scaling constant boosts intervention performance.

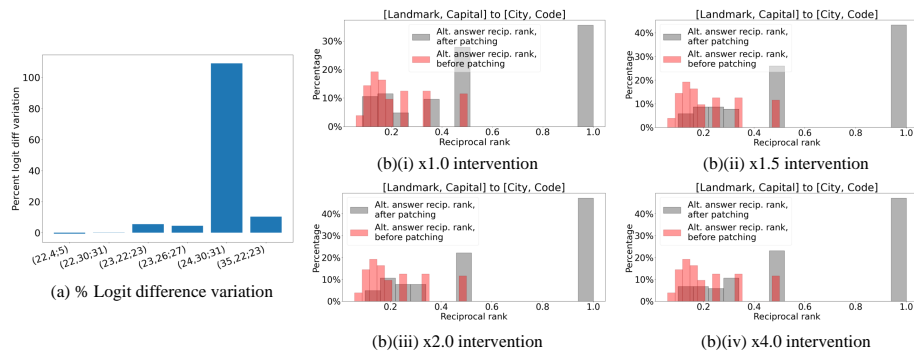


Figure 19: Gemma-2-27B [Landmark, Capital]→[City, Code] transfer experiments, intervening head groups (24, 30; 31), (35, 22; 23). We show the percentage logit-difference variation in (a), and reciprocal rank of the answer answer before and after intervention in the (b) series of figures, with different scaling constants in {1.0, 1.5, 2.0, 4.0}. We observe strong causal effects of the two attention head groups.

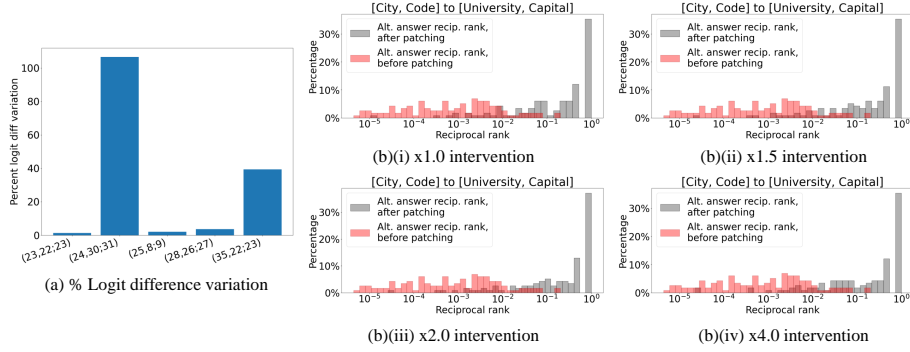


Figure 20: Gemma-2-27B [City, Calling Code]→[University, Capital] transfer experiments, intervening head groups (24, 30; 31), (35, 22; 23). At scaling constant 1.0 (i.e. natural intervention, no additional scaling), the reciprocal rank of 0.1 for the alternative answer after intervention is at the 36<sup>th</sup> percentile, while before patching, as we can see, the reciprocal rank of the alternative answer is mainly in the range of  $10^{-2}$  to  $10^{-5}$ .

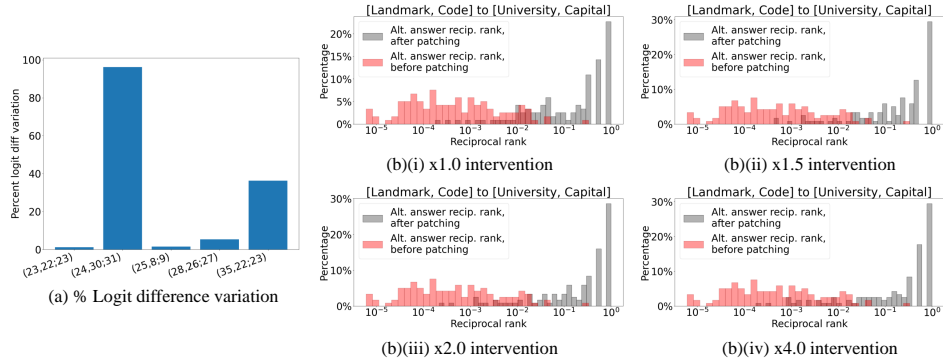


Figure 21: Gemma-2-27B [Landmark, Calling Code]→[University, Capital] transfer experiments, intervening head groups (24, 30; 31), (35, 22; 23). At scaling constant 1.0 (i.e. natural intervention, no additional scaling), the reciprocal rank of 0.1 for the alternative answer after intervention is at the 41<sup>th</sup> percentile.

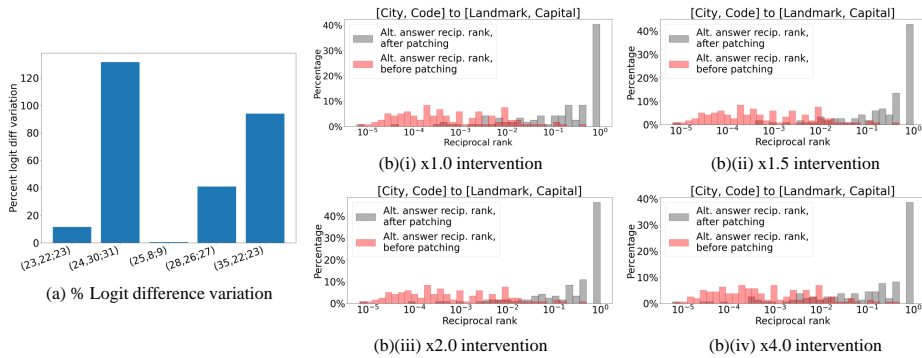


Figure 22: Gemma-2-27B [City, Calling Code]→[Landmark, Capital] transfer experiments, intervening the single head group (24, 30; 31). At scaling constant 1.0 (i.e. natural intervention, no additional scaling), the reciprocal rank of 0.1 for the alternative answer after intervention is at the 34<sup>th</sup> percentile.

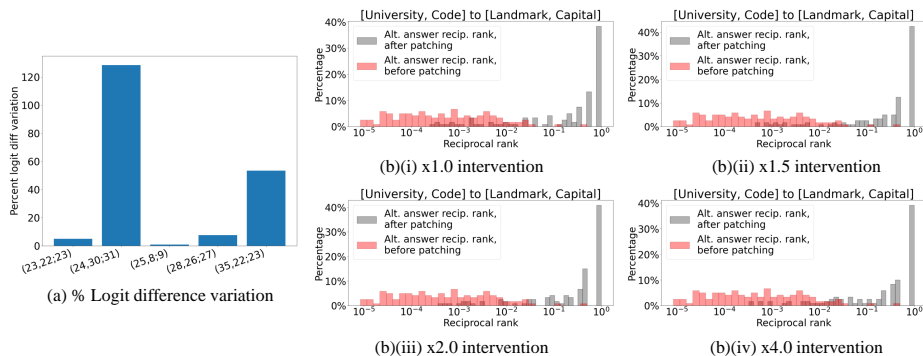


Figure 23: Gemma-2-27B [University, Calling Code]→[Landmark, Capital] transfer experiments, intervening the single head group (24, 30; 31). At scaling constant 1.0 (i.e. natural intervention, no additional scaling), the reciprocal rank of 0.1 for the alternative answer after intervention is at the 31<sup>st</sup> percentile.

though the target types have no overlap in text, perhaps the model still assigns nontrivial confidence to the “Capital” version of the alternative answer (which has target type “Calling Code”)? If that is so, then it challenges our hypothesis about the role of the “bridge” representations, since we might just be directly injecting the right version of the alternative answer into the model.

We show evidence to refute this. In particular, in Figure 26, we show that the model places trivial confidence on the altered-type answer, even if they share the same bridge value. Therefore, we add further evidence to the bridge-resolving mechanism.

**The role of MLPs.** We performed similar intervention experiments on the MLPs at the last token position just like with the attention heads. They are observed to be much less interesting in their functional roles: we find that the MLPs appear to primarily process the output concept type, and do not participate heavily in outputting the bridge concept representation. This is revealed in Figure 27.

**Smaller LLM exhibits weaker disentanglement.** To contrast against our results for the 27B model, we study a small model in the same family of Gemma 2 models, *Gemma-2-2B*. This smaller model has significantly lower accuracies on the problems, measured at 20 shots. [City, Capital]: 71.67%, [University, Capital]: 25.83%, [Landmark, Capital]: 66.67%, [City, Calling Code]: 47.5%, [University, Calling Code]: 57.5%, [Landmark, Calling Code]: 23.33%.

We perform an intervention experiment [University, Code]→[City, Capital] on *Gemma-2-2B*, similar to the bridge-resolving head localization experiments we did on the 27B model. Intriguingly, we were also able to surface a highly sparse set of attention heads which have nontrivial causal scores (but much lower than that achieved by the 27B model). We find that these heads exhibit noticeable, but *noisy* disentanglement with respect to the bridge representation. We show these results in Figure 28. The weaker causal score of the bridge-resolving heads and their noisier concept disentanglement in the 2B model suggests the conjecture that, the larger the model, the more specialized its concept-processing components are — assuming that the model is well-trained. Such specialization likely benefits the model’s generalization accuracy.

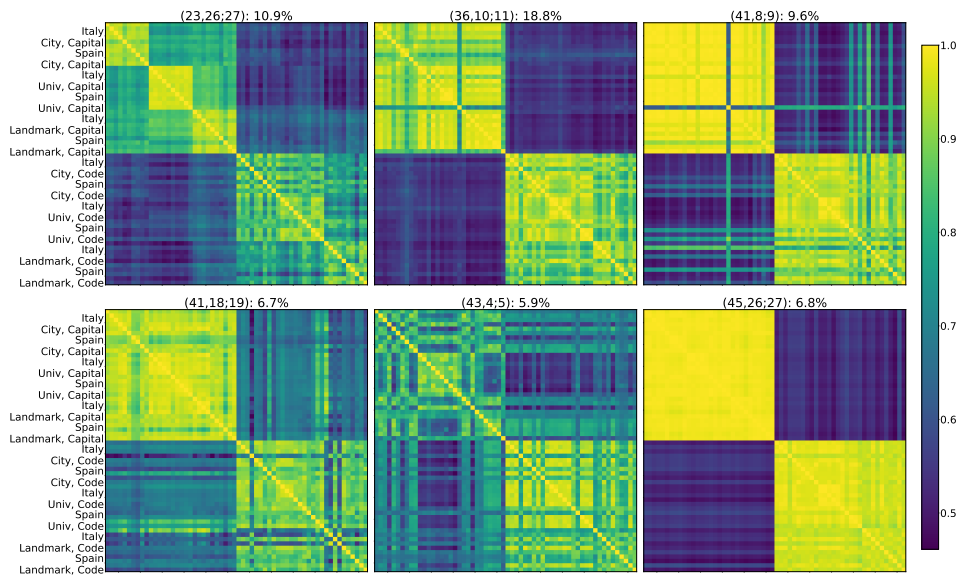


Figure 24: (Best viewed zoomed in) Cosine similarity map of the output-concept head groups (with top causal scores) identified in Gemma-2-27B, along with the percent logit-difference variation of the head groups, serving as the metric for the head groups’ causal effects. Observe that they are mostly insensitive to the source type, query value, and bridge value, and primarily sensitive to the output/target type. Note: in this set of visualizations, we are using “Italy” and “Spain” as the bridge values.

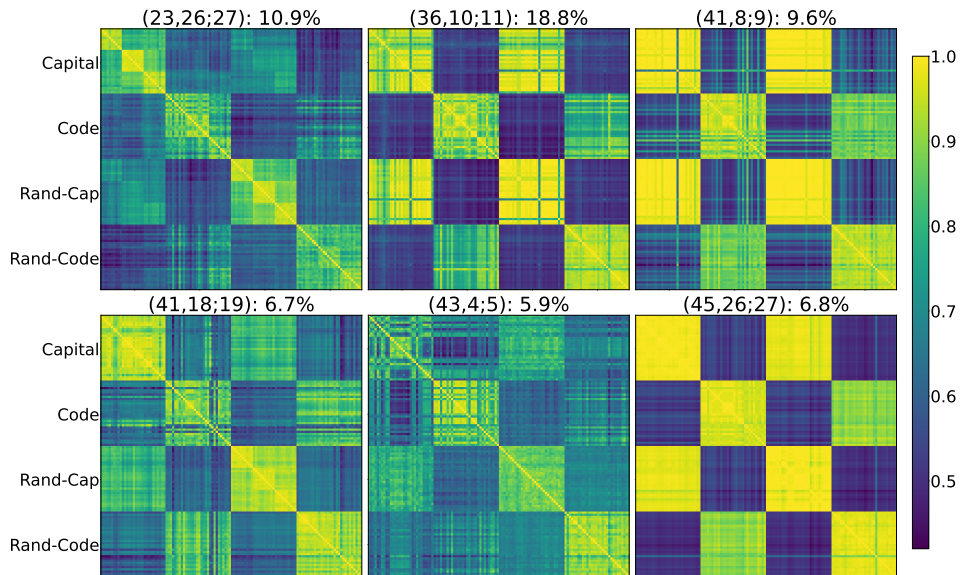


Figure 25: Cosine similarity map of the output-concept head groups identified in Gemma-2-27B. Here, we construct four groups of prompts. The first two groups consist of multi-hop ICL problems with Capital or Calling Code as the target type. The remaining two are created by randomly shuffling the output of the normal multi-hop ICL samples, causing the problem to essentially demand randomly outputting a Capital or a Calling Code; these are the “negative controls” we discussed in the main text. We find the output-concept heads’ embeddings on the multi-hop prompts to align strongly with those on the output-concept-only prompts, further confirming their role in the circuit.

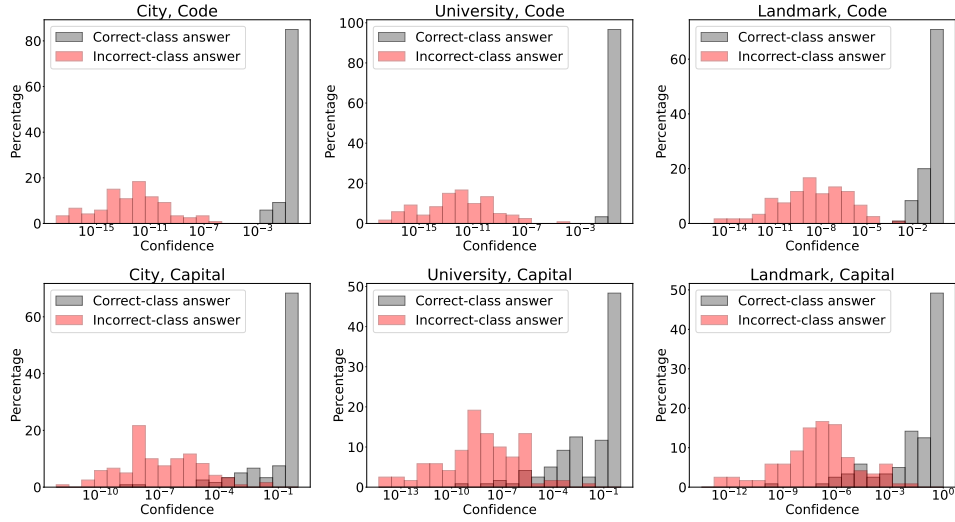


Figure 26: Distribution of Gemma-2-27B’s confidence on the correct- and incorrect-type answer on the different problems. When we say “correct-class” answer, we simply mean that the answer’s semantic type aligns with that of the problem’s target, e.g. the correct-type answer for a prompt “Okinawa, Tokyo. Nantes, Paris. ... Shanghai, ” would be “Beijing”, while the incorrect-type answer would be “1” (the calling code of China, which the city Shanghai belongs to). We observe a clear separation in the LLM’s confidence between the two types of answers.

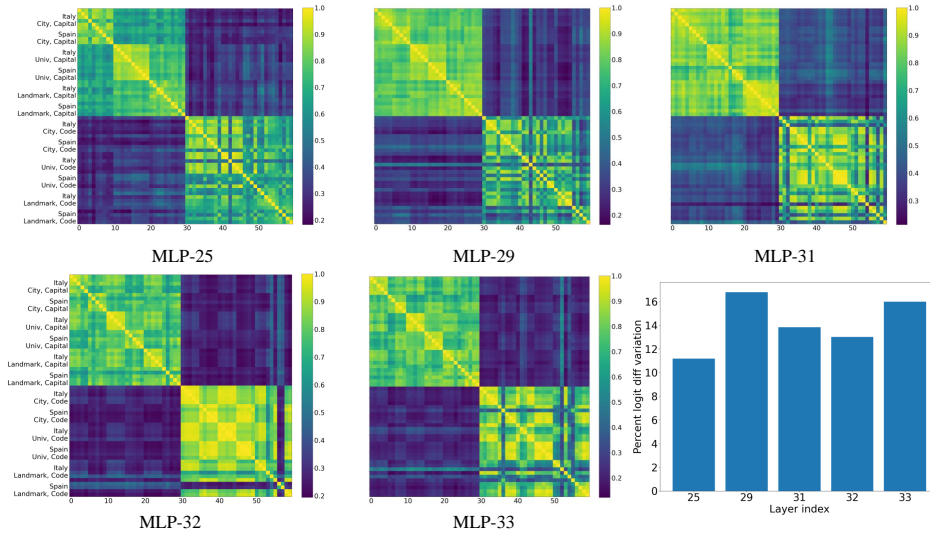


Figure 27: Functional roles of the MLPs in Gemma-2-27B. We perform patching experiments on [University, Code]→[City, Capital] at the last token position, similar to how we localize the bridge-resolving attention heads. We report the percentage logit-difference variation of the top-scoring MLPs, along with their cosine similarity maps computed on prompts sampled with different combinations of bridge values (“Italy” and “Spain”) and diverse set of source-target types. Perhaps unsurprisingly, the MLPs at the last token position play a less interesting role: as seen in the cosine similarity maps for the MLPs with the highest causal scores (fairly low compared to the attention heads), they primarily discriminate against the output type. They do not appear to participate much in resolving the bridge concept.

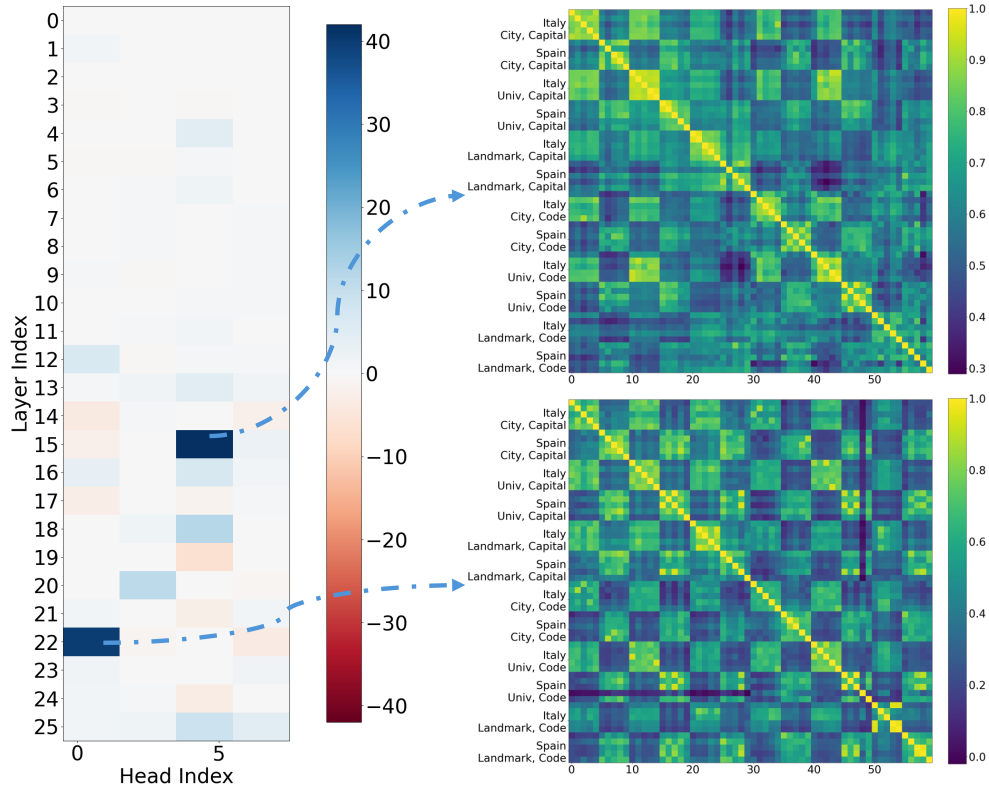


Figure 28: Results of the intervention experiment  $[\text{University, Code}] \rightarrow [\text{City, Capital}]$ , conducted on Gemma-2-2B, with 20-shot ICL. On the left, we show the percentage logit difference variation of the intervention experiment; on the right, we plot the cosine similarity map of the two head groups with the highest causal scores, namely (15, 4; 5) and (22, 0; 1). We find that while the two attention head groups exhibit nontrivial causal effects and disentanglement, they are, in comparison, much weaker than those exhibited by the 27B model. This likely explains the significantly lower accuracy of the 2B model than the 27B model. This also suggests a conjecture: perhaps the larger the model, the more specialized its concept-processing components are?

### A.3 The Company Puzzles, Another Multi-Hop ICL Task

**Problem setup.** To complement our study on the Geography puzzles and for more generality of our conclusion that sufficiently capable LLMs solve simple 2-hop ICL problems by resolving the bridge entities first, we work with another set of problems on globally well-known companies in the world. We collect data on 36 of them.

Here, our evidence is provided on a narrower range of source and target entity types, due to the nature of the problem. In particular, we allow source entities to fall in {Products, Founders}, and target entities to fall into {Founders, Headquarters City}. Furthermore, to obtain causal evidence that the model is resolving the bridge values from the query before producing the actual answer, we perform patching experiments with [Products, Founders]→[Founders, HQ City] and [Founders, Products]→[Products, HQ City]. If we again observe that there is high rank of the alternative prompt’s *converted* answer after patching a sparse set of attention heads on the final token position, then we see significant causal evidence that the model resolves the bridge value during inference.

Some manual cleaning was needed in creating this dataset, on top of ChatGPT sampling: we primarily filter out products which had company names in them, and companies whose products mostly contain the company name. An example category of this would be banks and credit/debit card services, e.g. Visa, Mastercard, HSBC, etc. For companies with multiple headquarters, we choose the most well-known one out of them as the correct “Headquarter City” of the company; this sometimes counts an old headquarter of the company as the correct one. *Note that this causes us to under-estimate the LLM’s accuracy with and without intervention!*

**Quantitative results.** We primarily work with the 16-shot ICL setting due to limited compute. In this setting, the [Product, Founder], [Product, HQ City] and [Founder, HQ City] have accuracies 73.5%, 80.7%, 88.6% respectively. We wish to note that this set of puzzles does rely on significantly more obscure knowledge than the Geography puzzles, so lower accuracies and weaker multi-hop links are expected overall.<sup>6</sup>

As Figures 29, 30 and 31 show, we again obtain evidence for the bridge-resolving heads. In particular, we find that head groups (22, 2; 3), (24, 14; 15), (24, 30; 31), (28, 12; 13), (28, 26; 27), (35, 22; 23) (0.8% of the total number of attention heads) exhibit the strongest causal effects in our experiments, and their output representations exhibit strong disentanglement with respect to the companies.

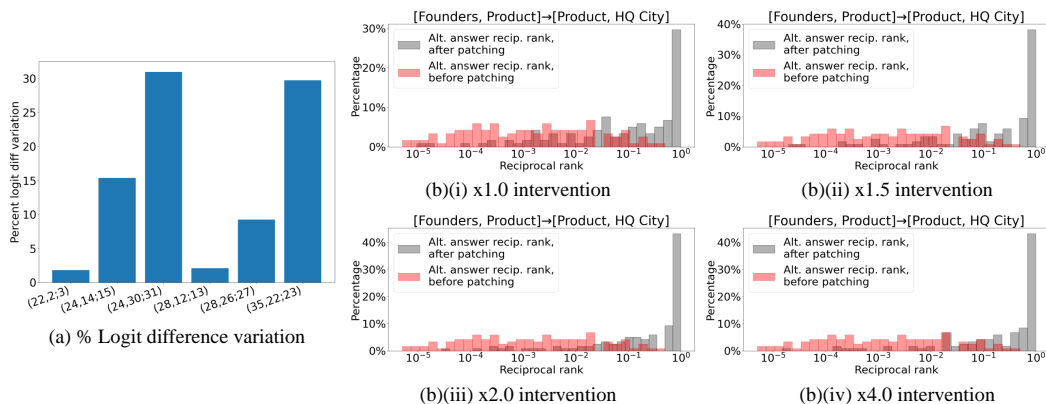


Figure 29: [Founder, Product]→[Product, HQ City] transfer experiments, intervening the head groups (22, 2; 3), (24, 14; 15), (24, 30; 31), (28, 12; 13), (28, 26; 27), (35, 22; 23) (0.8% of the total number of attention heads).

<sup>6</sup>We suspect that lower accuracy is not only due to the more obscure entities in this problem, but also because of several ambiguities. For example, (1) Product names are oftentimes simply not presented alongside company names, e.g. “Gatorade” is often not written alongside “PepsiCo”; (2) There can be confusion between company founders and well-known product directors, especially in certain art/entertainment companies.

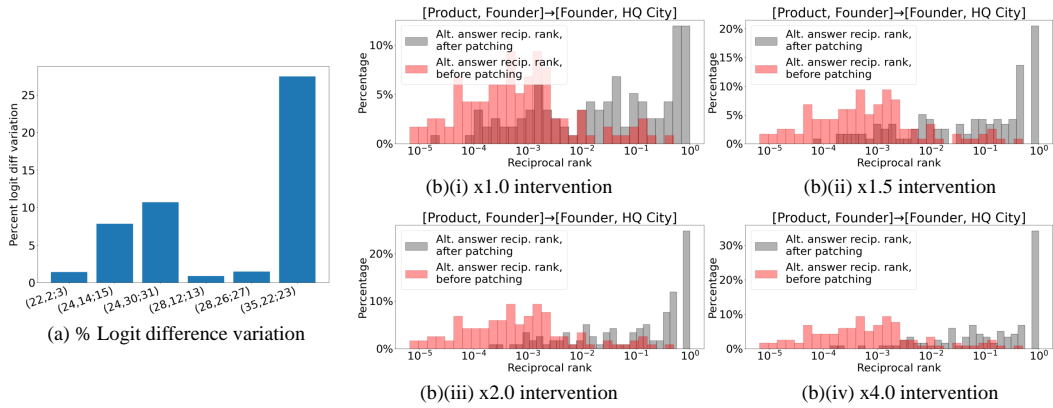


Figure 30: [Product, Founder]→[Founder, HQ City] transfer experiments, intervening the head groups (22, 2; 3), (24, 14; 15), (24, 30; 31), (28, 12; 13), (28, 26; 27), (35, 22; 23) (0.8% of the total number of attention heads).

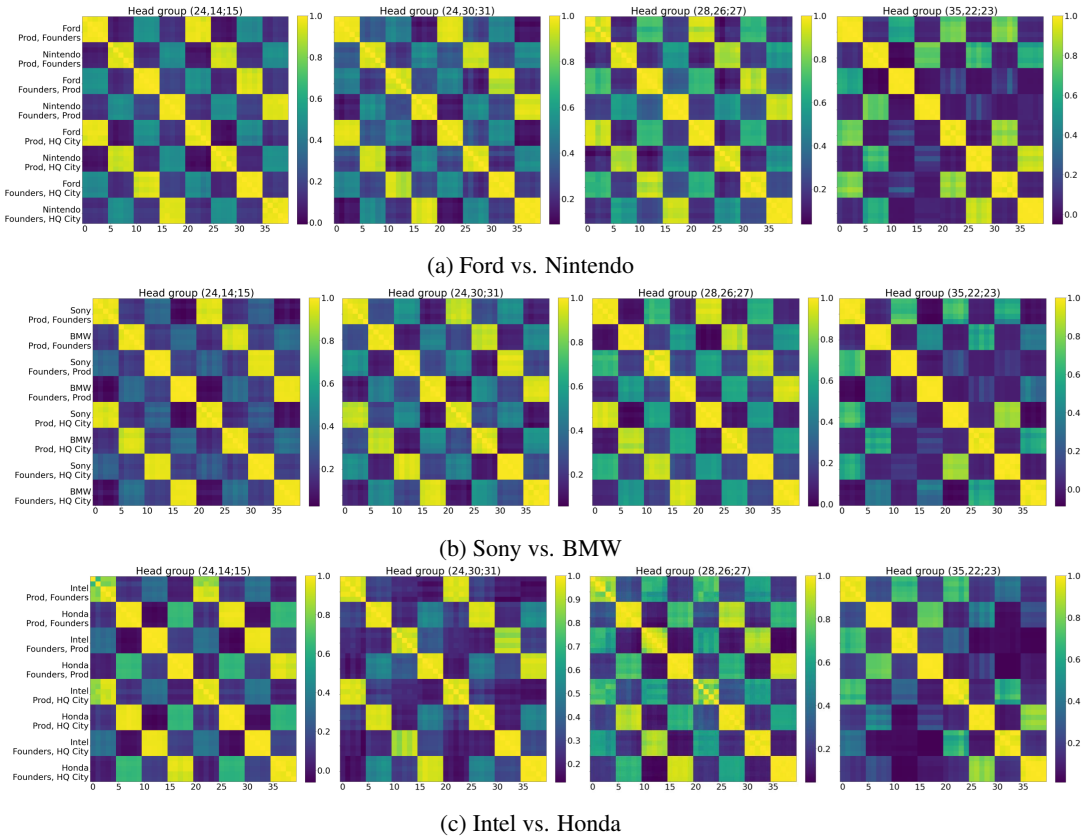


Figure 31: Cosine similarity of representations from the top-4 attention heads for resolving the bridge entity in Company ICL problems. For each combination of Bridge choice and source-target type, we sample 5 prompts to compare representation similarity on. We notice that the heads exhibit disentanglement with respect to the bridge concepts (the companies), but individually, they are not as capable in clearly resolving the bridge concepts in the Company problems as they do on the easier Geography problems (the latter problem having relevant accessible knowledge on many more websites than the former). This likely explains the model’s lower accuracies and somewhat weaker intervention results on the Company problems, compared to the Geography problems.

## B Experimental Details and Additional Experiments for Section 3

This section includes experimental details and additional experiments for problems with numerical or continuous parameterization considered in Section 3.

**Compute.** The experiments in this section were performed on an internal cluster with a P100 and a V100 GPU. We list training details such as batch sizes and iterations used for the experiments in their respective sections.

### B.1 More on the add- $k$ Problem

In this section, we investigate the effect of increasing the number of tasks on the results shown in Fig. 8, where we showed that the task vectors for  $K = 4, 8, 16$  offsets lie on a 1D linear manifold. In these settings, the model reached  $\approx 100\%$  train and test accuracy.

We consider a setting with 32 offsets with gap between the offsets  $k_{i+1} - k_i = 1$ . In this setting, the train/test accuracies reach only about 90%, which indicates this is a harder problem for the model to solve. Fig. 32 shows 3D and 2D PCA projections of the task vectors. These explain about 96.1% and 84.48% of the variance, respectively. We see that the task vectors lie on a 3D manifold that looks like a (small) helix, with alternating (odd and even) offsets represented in two separate arcs of the helix. This is significantly different from the 1D linear manifold we observed with a smaller number of offsets in Fig. 8. This type of geometry is reminiscent of the observations in Zhou et al. [56], Kantamneni and Tegmark [57], which study how pre-trained language models do addition and find that these models encode numbers as a helix.

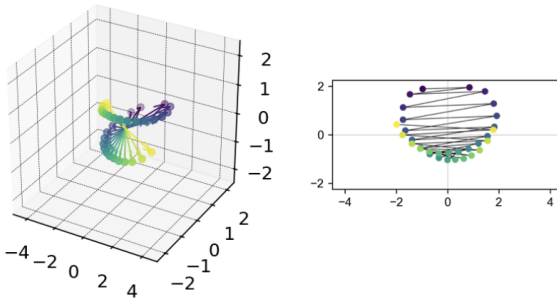


Figure 32: 3D (left) and 2D (right) PCA projections of the task vectors for the *add- $k$*  problem with 32 offsets. The task vectors lie on a 3D manifold that looks like a (small) helix. From the 2D projection, we see that alternating (odd and even) offsets are represented in two separate arcs of the helix.

**Training Details.** The models were trained for 1000 iterations using AdamW optimizer with learning rate 0.001 and weight decay 0.01. We use a linear learning-rate schedule with a warm-up phase over the first 10% iterations. The train data contains  $5000K$  sequences, we use a batch size of 500 for  $K = 4, 8, 16$ , and 2000 for  $K = 32$ .

### B.2 More on the Circular-Trajectory Problem

In this section, we include further details about the experimental setup of the Circular-Trajectory problem, and present some additional results.

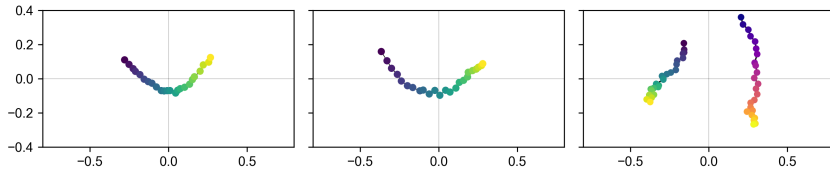


Figure 33: 2D projection of task vectors for the Circular-Trajectory problem when the model is trained on 32 radius values. The three plots show task vectors for clockwise (CW) trajectories, counterclockwise (CCW) trajectories, and all trajectories considered together, respectively. We observe that CW and CCW circle trajectories are represented on two manifolds in the 2D space.

In Fig. 10 in the paper, we show the geometry of task vectors for the Circular-Trajectory problem for sequences where  $c = -1$ , *i.e.*, the trajectories are clockwise (CW). In this section we look at

the geometry of task vectors for sequences with counterclockwise (CCW) trajectories, as well as all sequences considered together. In Fig. 33, we plot the 2D projection of task vectors for CW, CCW and both taken together, respectively. We consider 32 radius values while training. The variance explained by 2 PCs for the three plots is 93.55%, 96.32%, 89.1%, respectively. Darker colors correspond to smaller radius values, and the two colormaps in the third subplot represent CW or CCW trajectories. We observe that CW and CCW circle trajectories are represented on two manifolds in the 2D space.

**Training Details.** In this setting, we sample a new batch of sequences at every iteration. We use batch size 64 and train the model on a total of 200 000 sequences. We use Adam optimizer with learning rate  $10^{-4}$  and weight decay 0.001. We use representations at position  $\lfloor \frac{n}{2} \rfloor$  as the task vector following the process mentioned in Section 3.1, averaging over 100 sequences each. These settings remain the same for the experiments in the next section.

### B.3 More on the Rectangular-Trajectory Problem

In this section we consider a Rectangular-Trajectory problem, parameterized by two parameters, namely the lengths of the two sides of the rectangle, say  $(a, b)$ . Specifically, the trajectories contain points on axis-aligned rectangles centered at the origin. Let  $e$  denote the number of points on each edge of the rectangle spaced uniformly. The starting point of the sequence is randomly sampled from one of the  $e$  points on the right vertical edge of the rectangle. The rest of the points are obtained by traversing the rectangle CW or CCW, determined by  $c = -1$  or 1. Fig. 34 shows an example sequence.

Similar to Circular-Trajectory problem, each sequence is obtained by first sampling  $a$  and  $b$  uniformly between 1 and 4, then sampling the starting point and  $c = -1$  or 1, and then following the aforementioned process. For our experiments, we set  $e = 5$  and  $n = 15$  for this task. The number of tasks  $K$  denotes the number of different combinations  $(a, b)$ .

In Fig. 35, we plot the 2D projection of the task vectors obtained for all  $(a, b)$  combinations lying on the 2D grid between  $a \in [1, 4]$  and  $b \in [1, 4]$ . Similar to the experiments in Fig. 10, we plot the task vectors for trajectories with  $c = -1$  here. We consider  $K = 32$  in this experiment. The first two PCs explain 91.97% variance. We observe that all the task vectors lie on a 2D manifold.

This setting goes beyond the Circular-Trajectory problem and shows that transformers represent task vectors corresponding to the problem parameters (radius for circles and edge lengths for rectangles) in low-dimensional (smooth) manifolds in both cases.

## C Limitations and Broader Impact

There are a few limitations of this work, which we discuss below.

- We only look at English language queries for the Geography puzzles, so we do not evaluate how mechanisms may change across different languages. The input language may correlate with the model’s parametric knowledge that the model uses to recall the Bridge entity. A more thorough study would compare model mechanisms for prompts across several languages, to ensure that the results remain the same.
- The latent concepts that we test for all have easy to understand human representations, such as numbers, countries, or geometric shapes. This limits our study to a subset of possible latent concepts that could be present in the ICL examples. There may be other, more intricate, relationships between the ICL examples that the model is also representing in some way. It would be ideal to provide ablations over the human-interpretability of the provided examples, to see if this affects how the model represents the latent concepts.

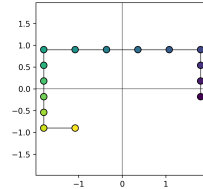


Figure 34: An illustration of a sequence of points for the Rectangular-Trajectory problem with  $e = 5$  points per edge, and  $n = 15$ . See text for details.

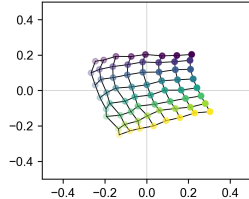


Figure 35: 2D projection of the task vectors obtained for 64  $(a, b)$  combinations. Fixed color or transparency level corresponds to fixed  $a$  or  $b$ , respectively. The task vectors lie on a (smooth) 2D manifold.